

# **Astr 511: Galaxies as galaxies**

Winter Quarter 2017, University of Washington

Mario Juric & Željko Ivezić

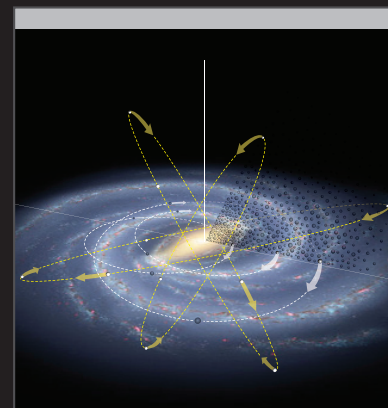
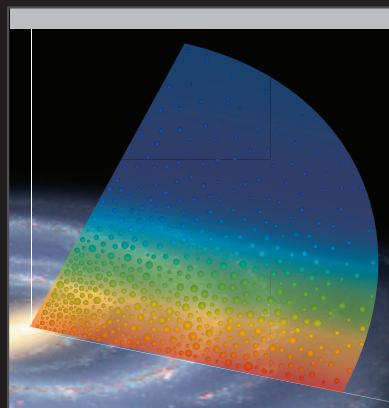
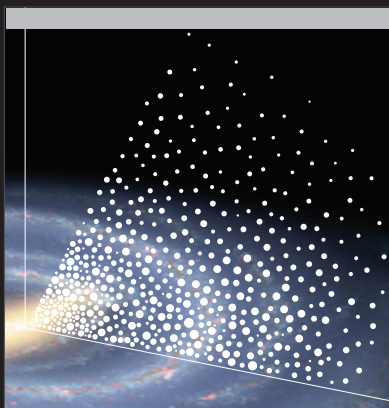
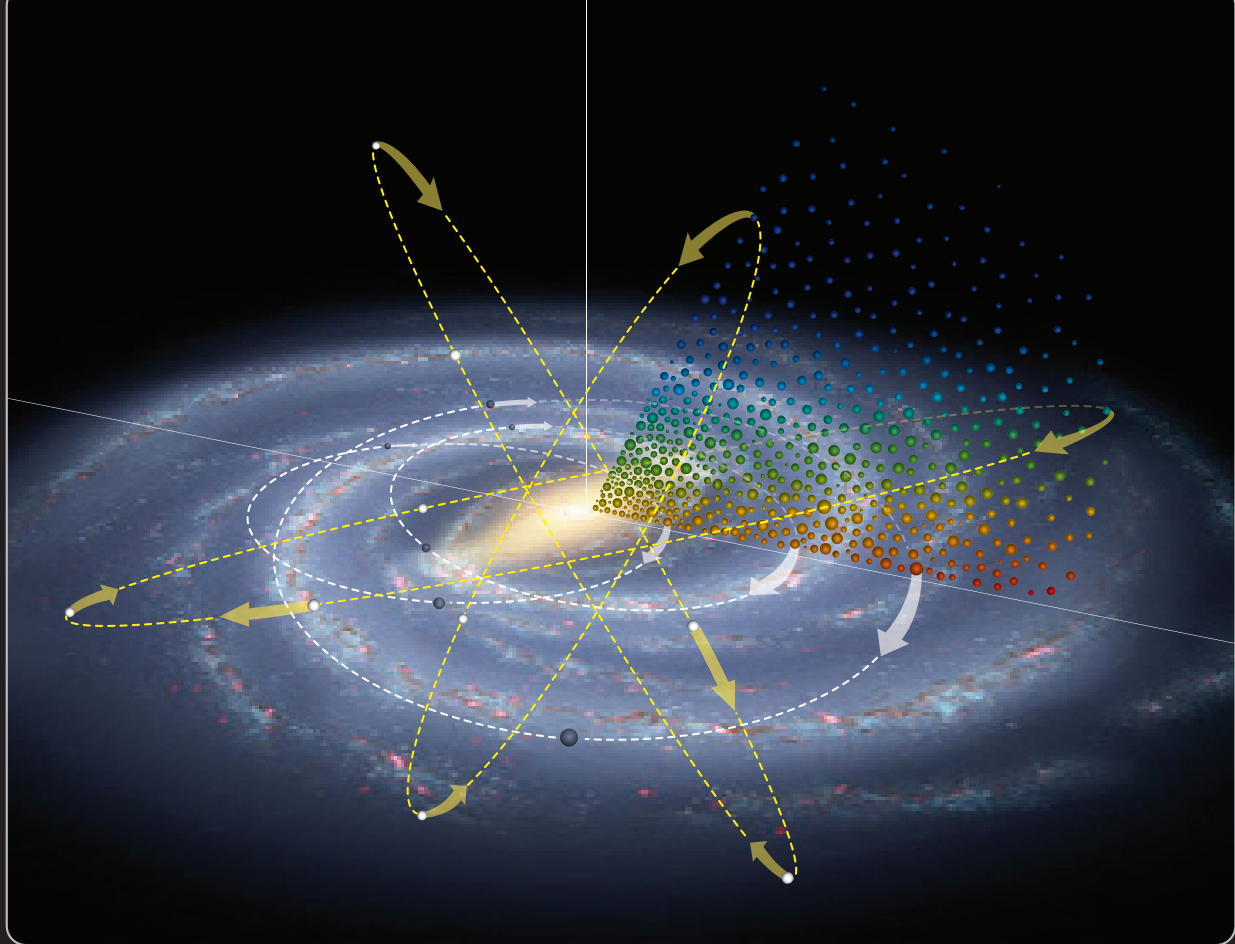
## Lecture 13:

Stellar metallicity and kinematics in the Milky Way

The three basic stellar distribution functions:

1. Number density
2. Metallicity
3. Kinematics

These three distribution functions provide observational constraints for the model selection (models for galaxy formation and evolution)



# Outline

1. Metallicity distribution: introduction, disk vs. halo
2. Stellar Kinematics: measurements
3. Stellar Kinematics: disk vs. halo

## Reading:

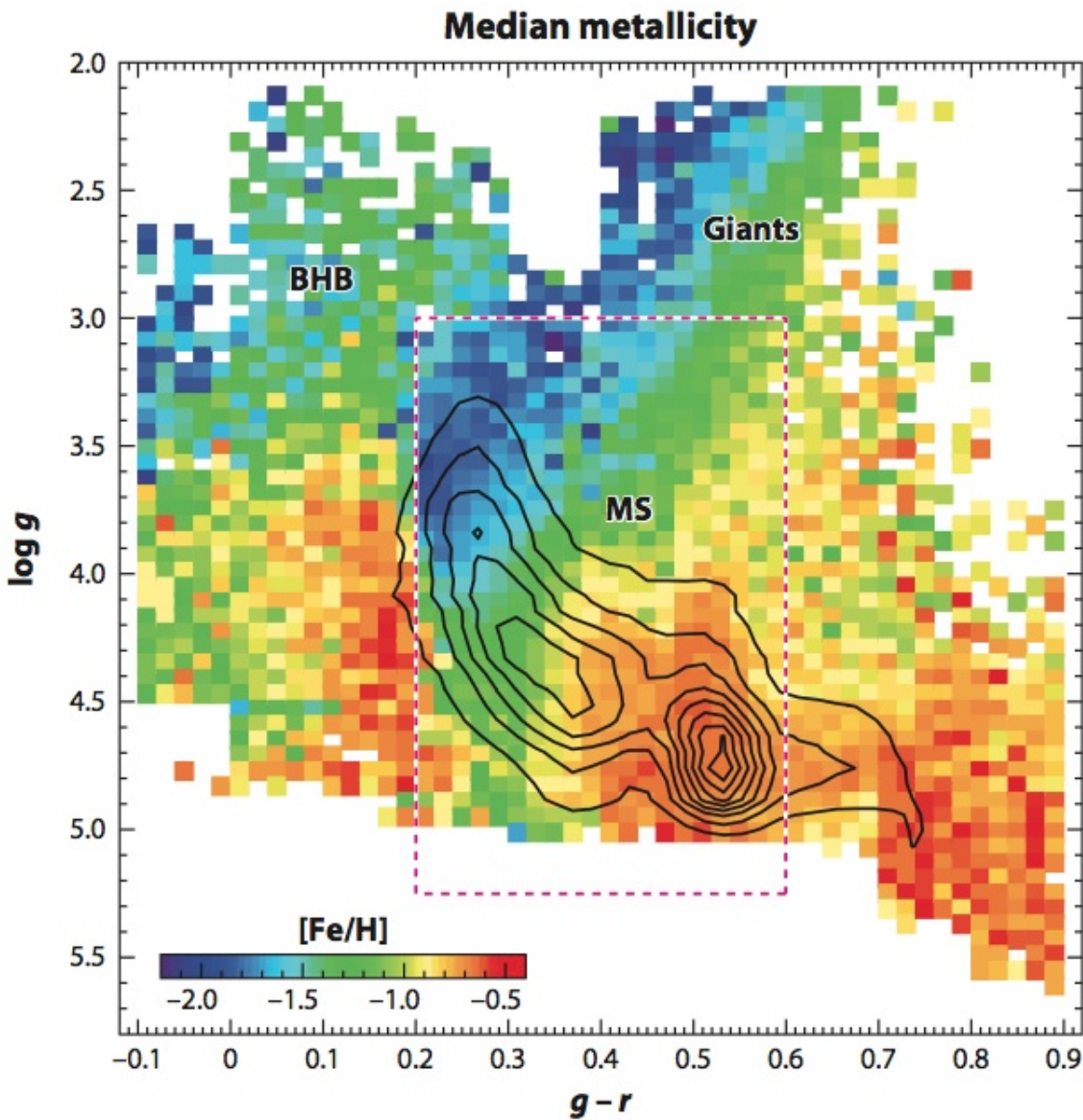
- Ivezić et al. 2008 (ApJ 684, 287): Sec. 3.4 and 4 at least
- Bond et al. 2010 (ApJ 716, 1): Sec. 1 to 6 at least
- Reid & Hawley: ch. 7 and 8; Binney & Merrifield: ch. 10

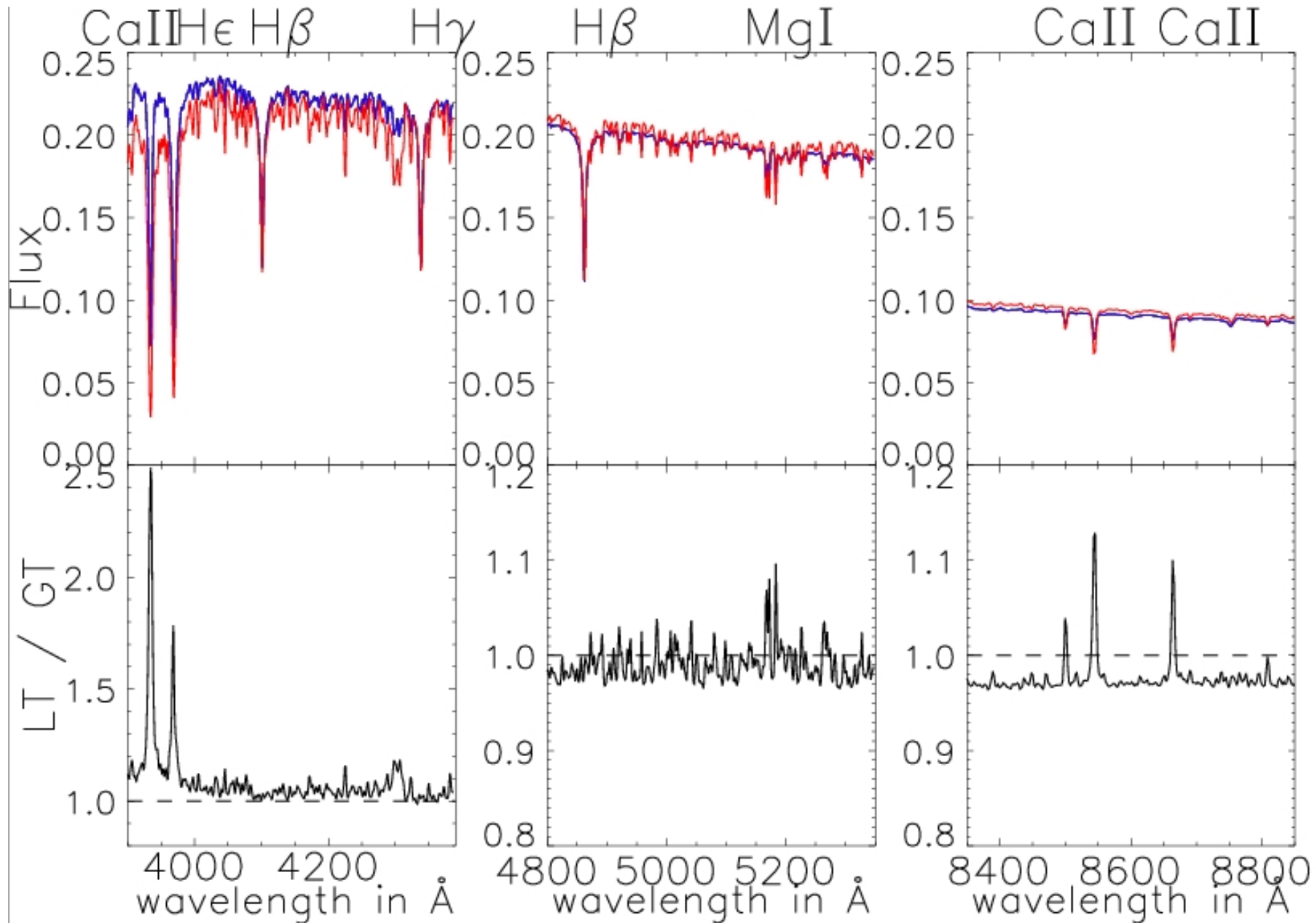
## Introduction: metallicity

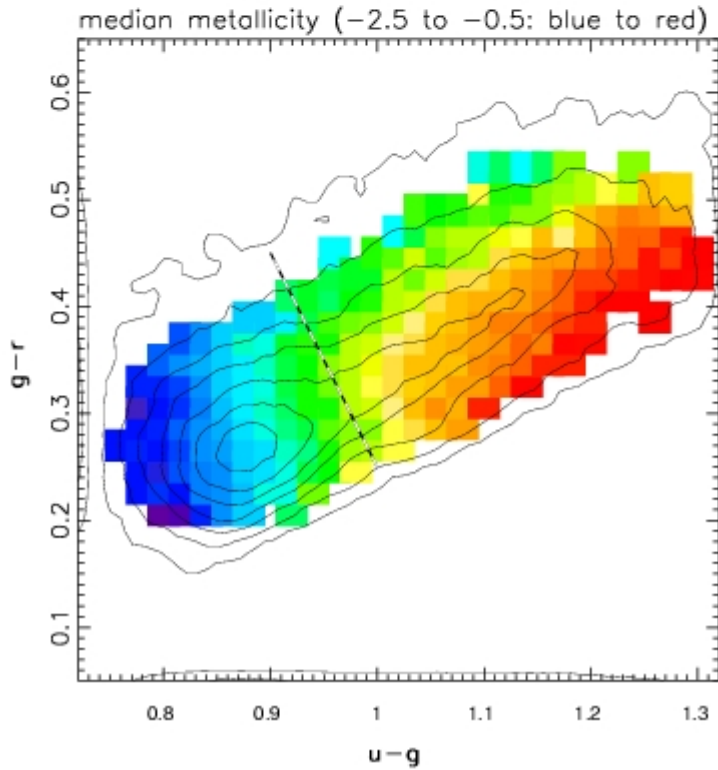
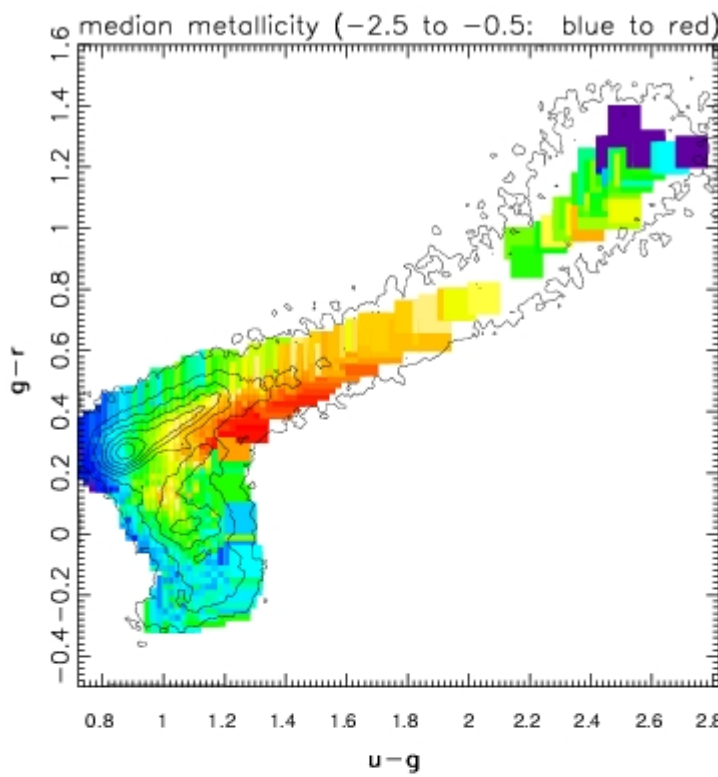
- Given the **mass fraction** of hydrogen,  $X$ , and the fraction of helium  $Y$ , the fraction of all the remaining chemical elements is  $Z = 1 - X - Y$ .
- For the Sun,  $X_{\odot} = 0.7381$ ,  $Y_{\odot} = 0.2485$  and  $Z_{\odot} = 0.0134$  (Asplund et al. 2009, ARA&A 47, 481).
- Metallicity is defined, using *the numbers of atoms*, as  $[Fe/H] = \log_{10} (N_{Fe}/N_H)_* - \log_{10} (N_{Fe}/N_H)_{\odot}$ .
- The following proportionality is usually assumed, with  $C \sim 1$  (to within 10% or so),  
$$[M/H] \equiv \log_{10} \left( \frac{Z_*/X_*}{Z_{\odot}/X_{\odot}} \right) = C [Fe/H].$$
- Confusingly, both  $[M/H]$  and  $[Fe/H]$  are called “metallicity”.

## Stellar Parameters Estimation

- SDSS stellar spectra are automatically processed to obtain stellar parameters such as **effective temperature, gravity, metallicity**.
- **Left:** resembles a warped HR diagram; the color-coded map shows the median metallicity as a function of  $\log(g)$  (roughly, dwarfs vs. giants) and the  $g-r$  color (roughly, effective temperature), according to the legend in the bottom left corner; the contours show the distribution of all SDSS stars with spectra (biased!)

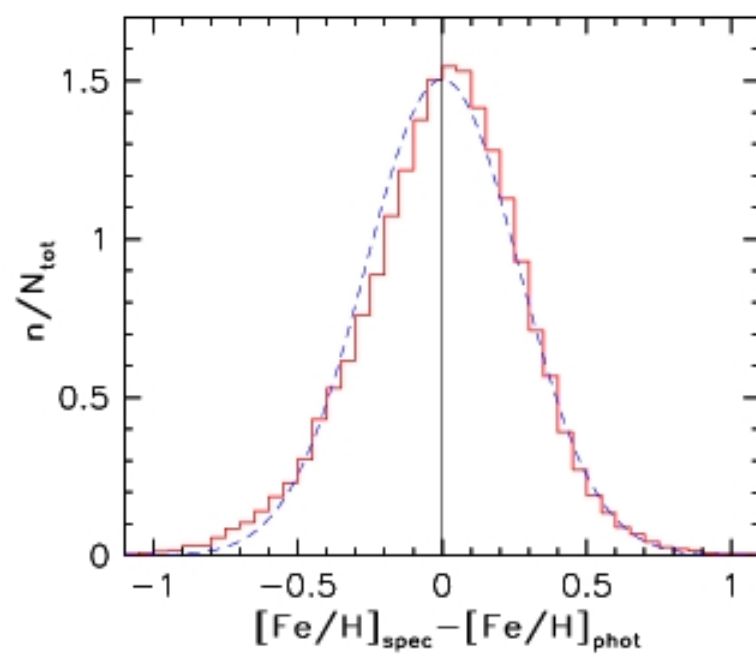
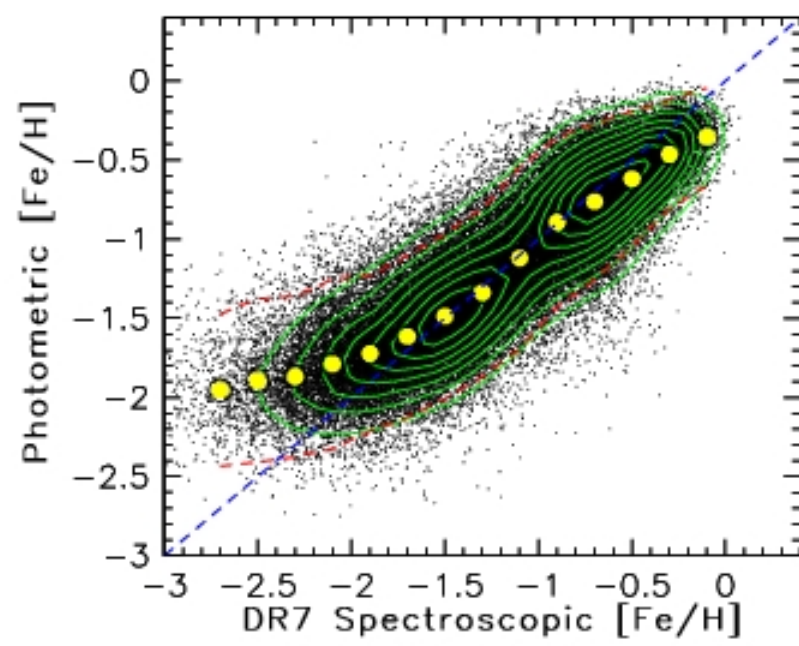
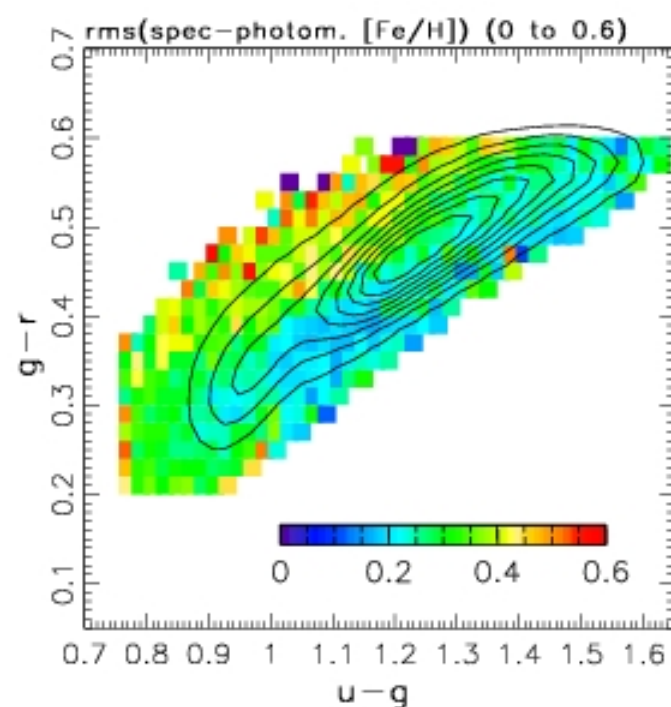
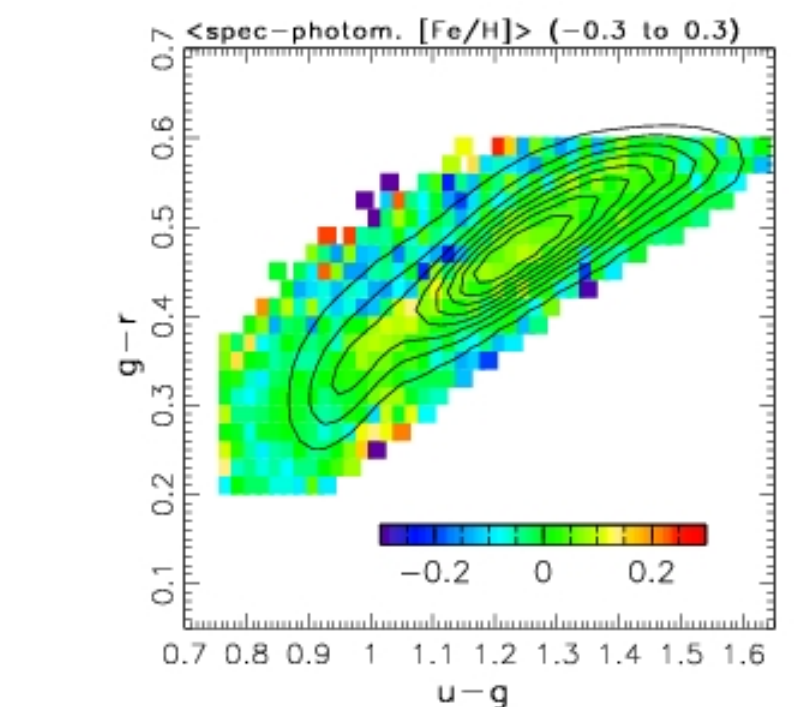






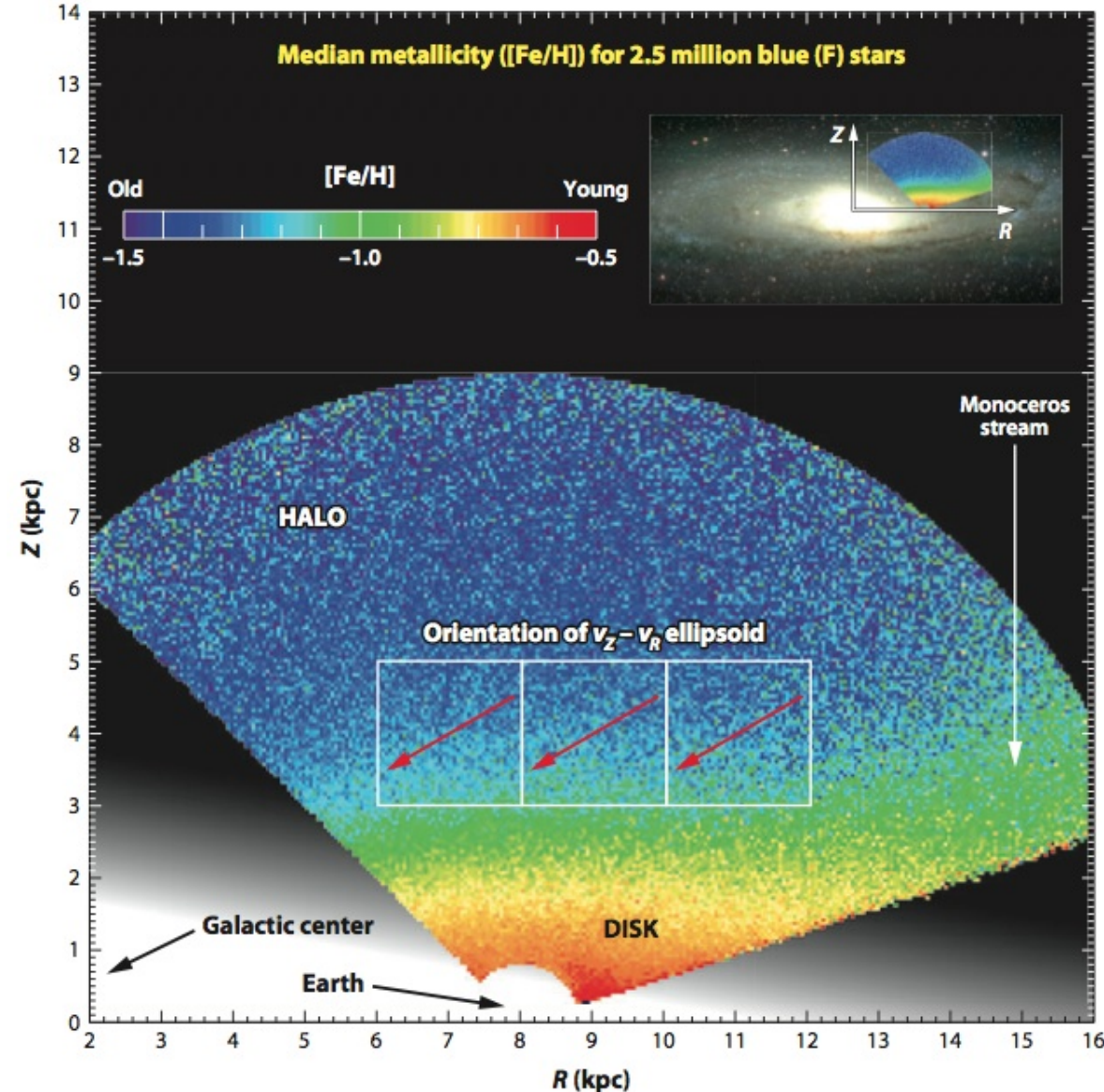
## Stellar Parameters Estimation: [Fe/H]

- Stellar parameters estimated from spectra show a good correlation with colors measured from imaging data
- **Top left:** the median metallicity as a function of the position in the  $g - r$  vs.  $u - g$  diagram ( $-0.5$  to  $-2.5$ , red to blue)
- **Bottom left:** zoomed-in version of the top left figure
- **Photometric estimate of metallicity:** can be determined with an error of  $\sim 0.2\text{--}0.3$  dex (relative to spectroscopic estimate) from the position in the  $g - r$  vs.  $u - g$  color-color diagram using simple expressions
- This finding is important for studies based on photometric data alone, and also demonstrates the robustness of parameters estimated from spectroscopic data



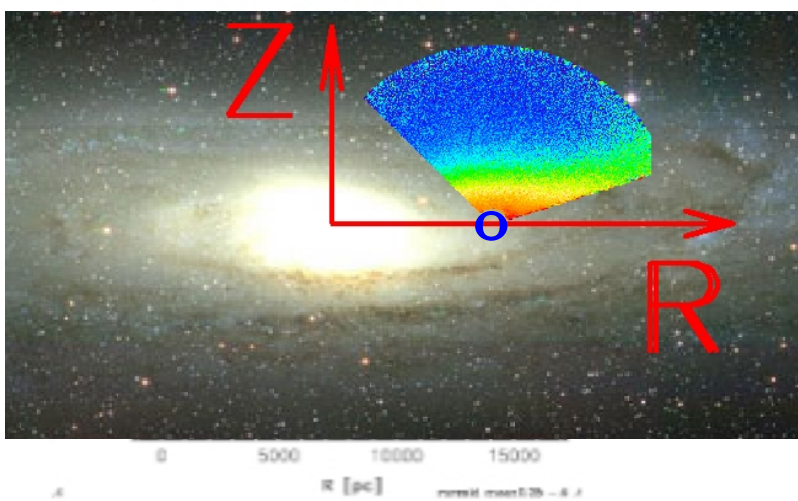
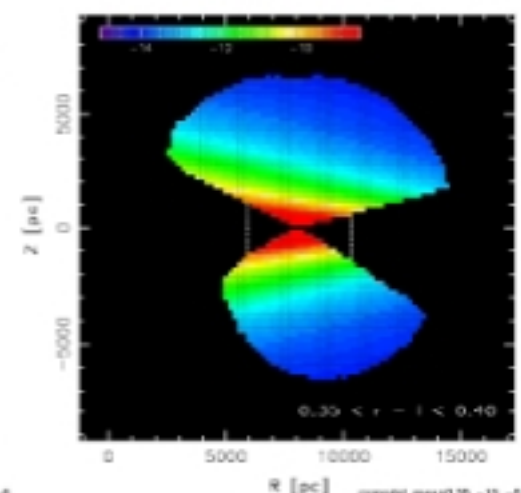
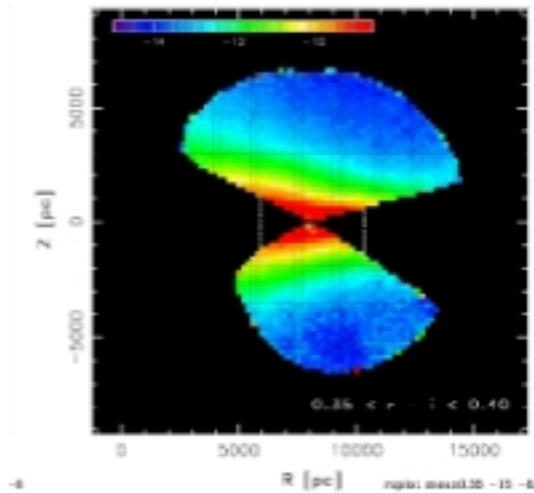
## Photometric Metallicity Distribution

- Panoramic view of the Milky Way metallicity distribution: the median metallicity map contains  $\sim 8,000$  pixels (0.1 kpc by 0.1 kpc), and is based on a complete flux- and color-limited sample of  $\sim 2.5$  million blue stars.
- The median metallicity is a strong function of distance from the Galactic plane; deviations are associated with spatial (and kinematic) substructures



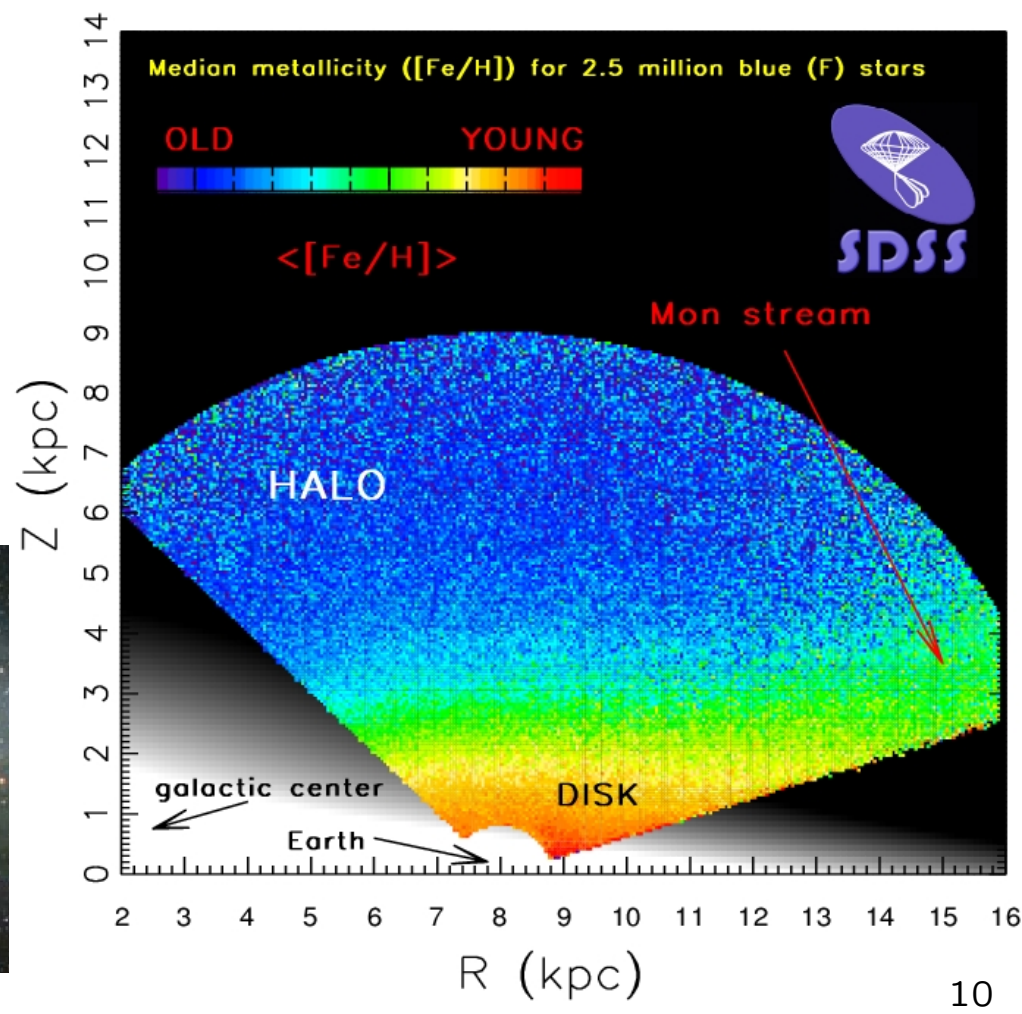
A harder analysis problem than counts; instead of a single count value, at each position there is a (scalar) distribution function,  $p([{\rm Fe/H}])!$

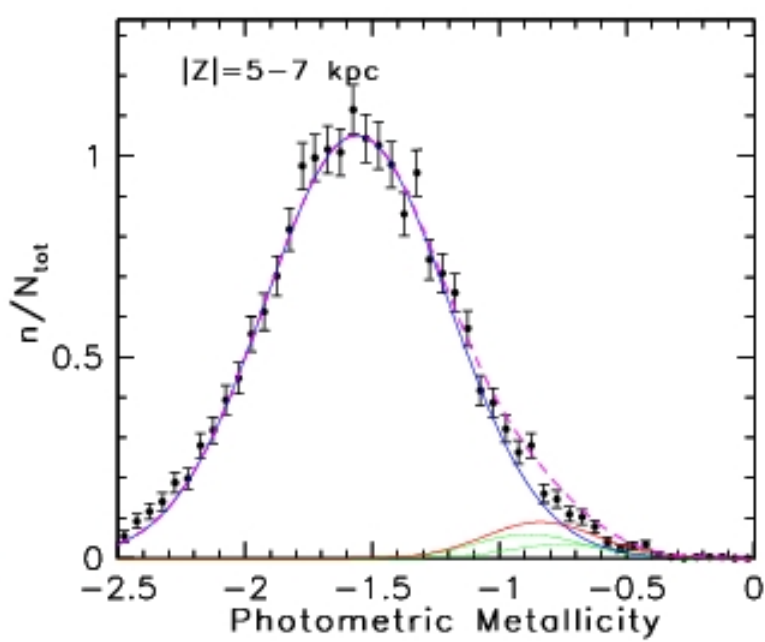
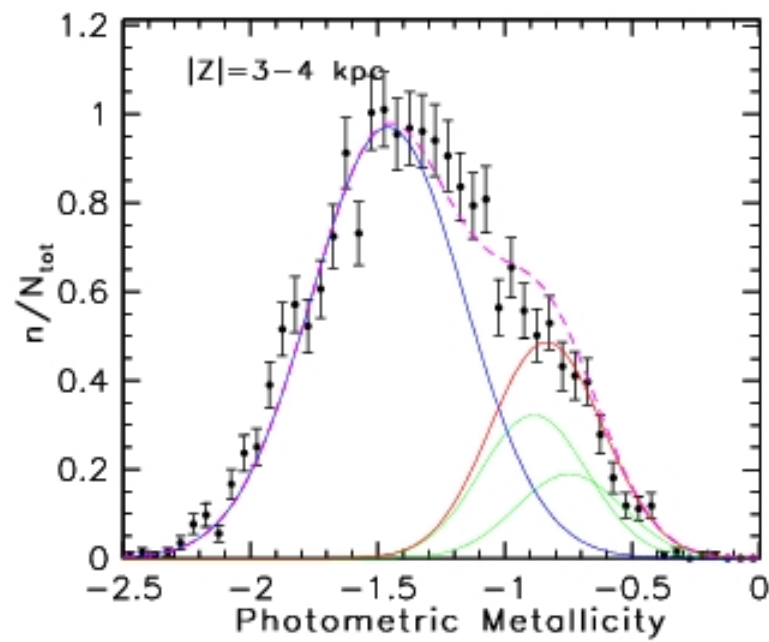
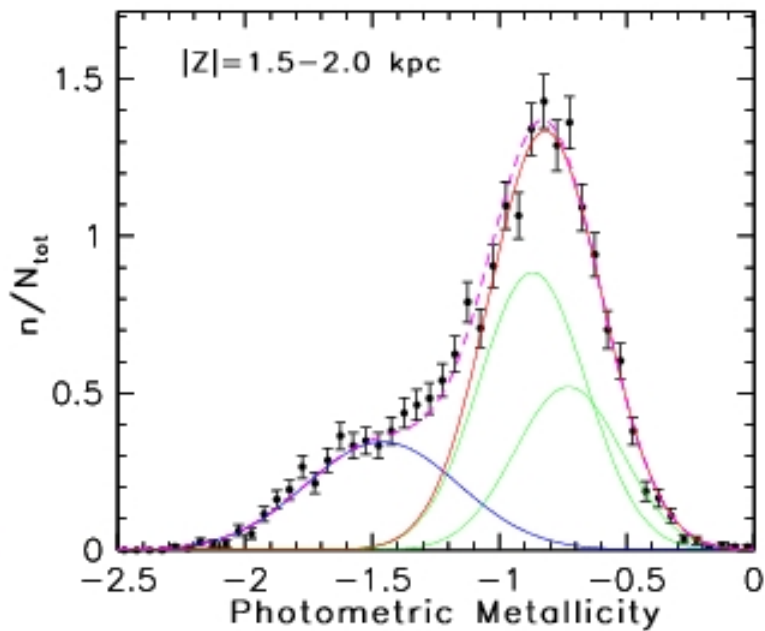
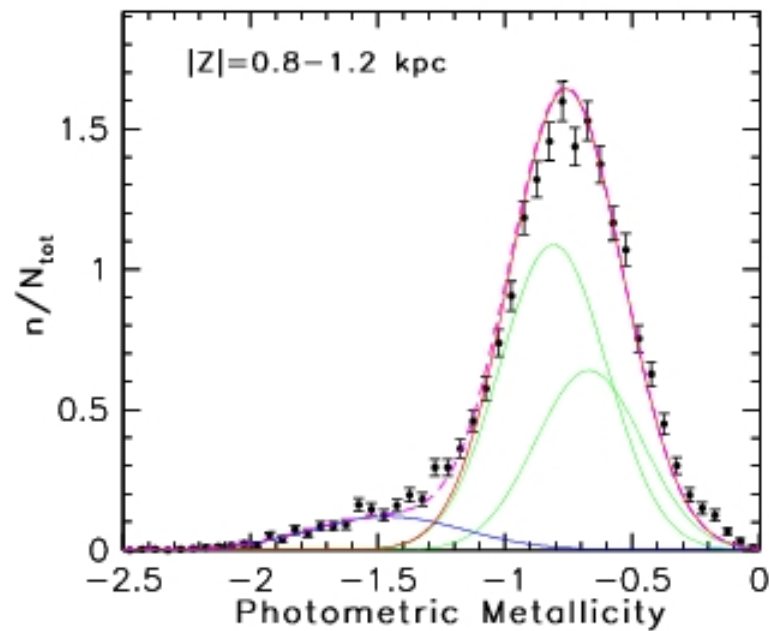
$0.35 < r-i < 0.40$

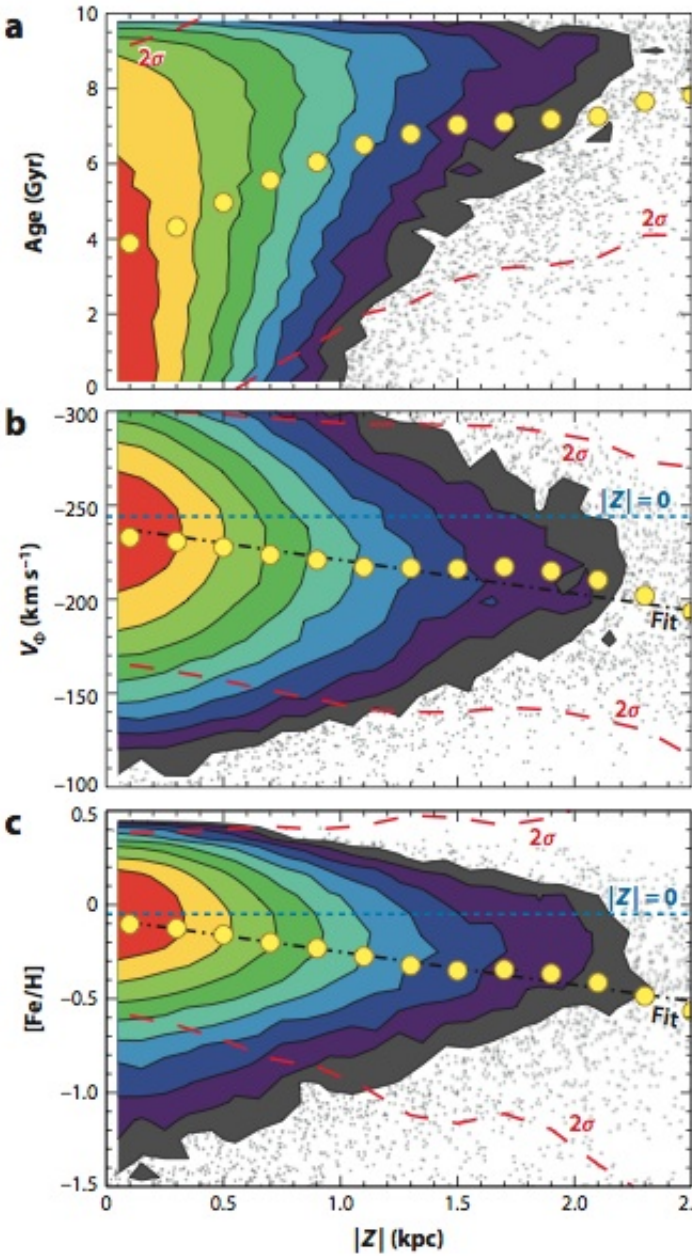


## Dissecting the Milky Way with SDSS

- Panoramic view of the Milky Way, akin to observations of external galaxies; **good support for standard Galactic models** (with amazing signal-to-noise!)
- **Metallicity mapping** supports components inferred from number counts mapping



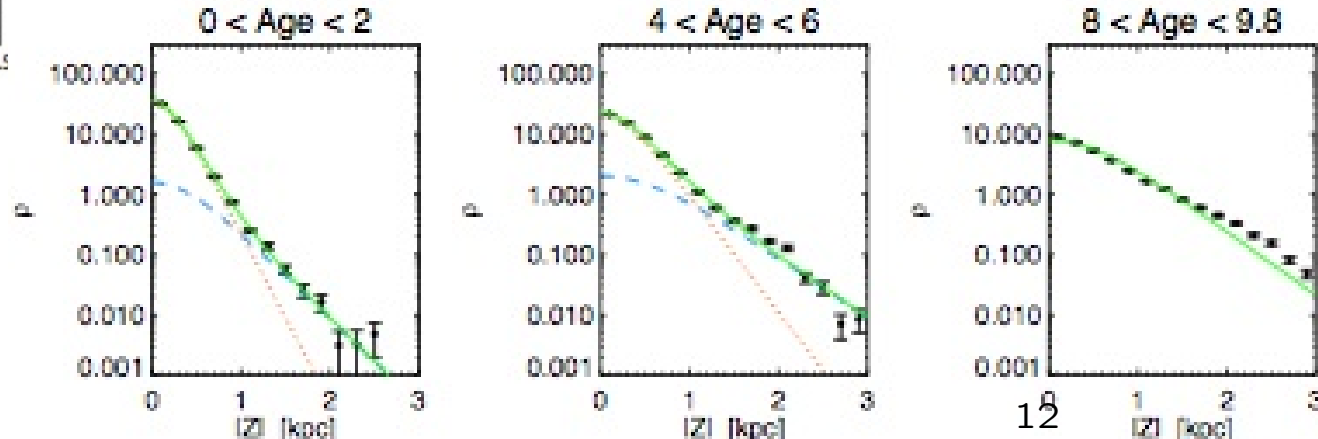


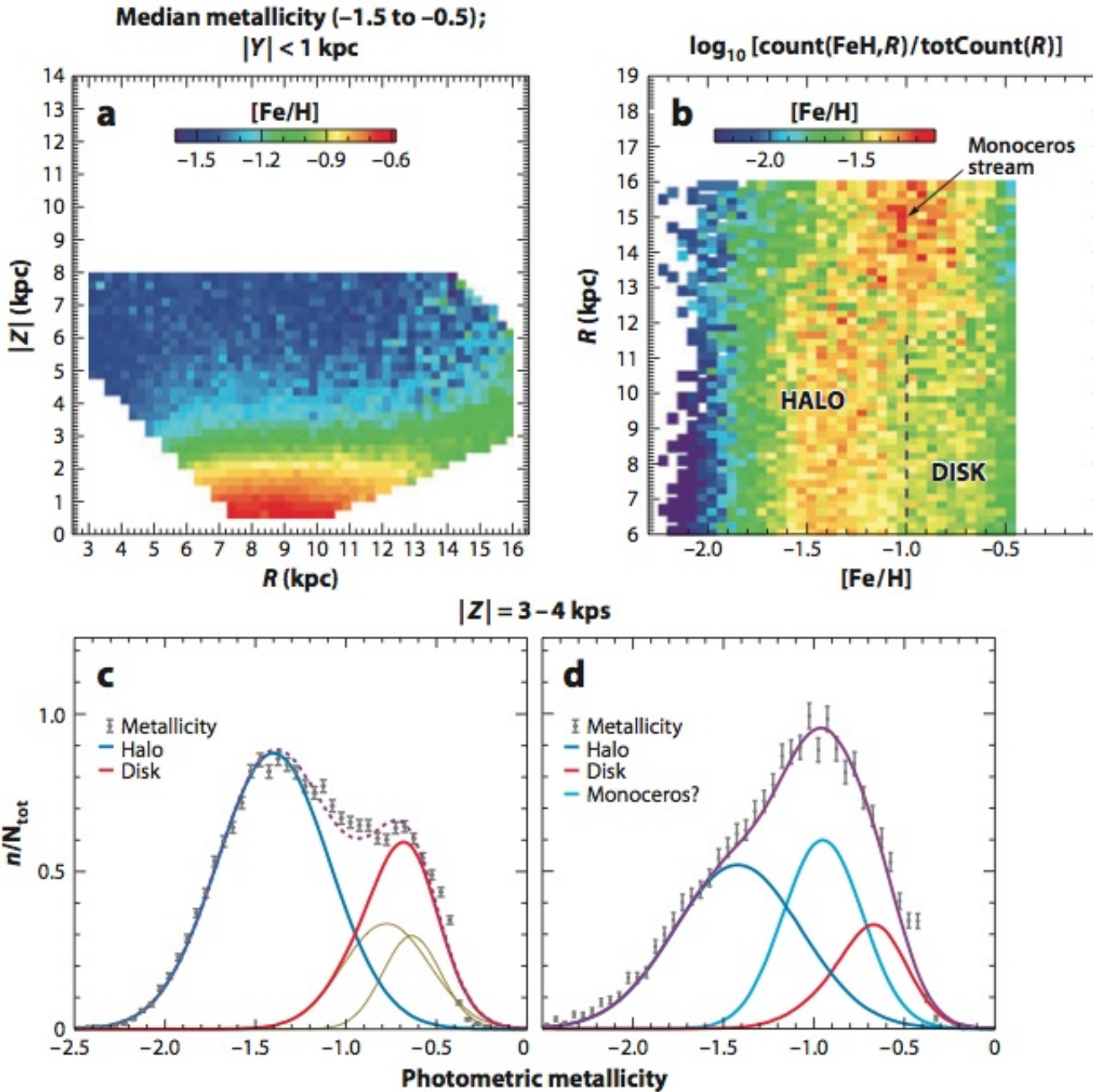


**Loebman et al. 2011**  
**(ApJ, 737, 17)**  
**(Roškar et al. models)**

## Is Thin/Thick Disk an Age Effect?

- **Data:** Change of slope of stellar counts at  $\sim 1$  kpc, and both rotational velocity distribution and metallicity distribution for disk stars vary with  $Z$
- N-body models with radial migration:
  - 1) behave like the data, and
  - 2) provide age information and details about radial migration
- **Models:** Older stars 1) reach larger  $|Z|$ , 2) have lower  $[Fe/H]$ , 3) display rotational velocity lag, 4) no  $[Fe/H]-v_\phi$  correlation **Observers call this behavior “thick disk”**





## Metallicity Substructure

- Monoceros stream was discovered using stellar counts
- It is also identified as a substructure in metallicity space... LEFT
- And kinematics, too: it rotates faster than LSR by  $\sim 50 \text{ km/s}$
- More details: Ivezić et al. 2008 (ApJ 684, 287)

**There is fine substructure in the metallicity distribution!**

## Introduction: $\alpha$ elements

- $\alpha$  elements are produced by the  $\alpha$  process, one of the two main nuclear fusion processes responsible for the production of heavy elements from helium (the other one is the triple  $\alpha$  process). Their most abundant isotopes are integer multiples of four ( $\alpha$  particle is the helium nucleus) and have atomic number up to 22.
- $\alpha$  elements include O, Ne, Mg, Si, S, Ar, Ca, Ti.
- $\alpha$  elements are important for understanding the star formation history because Type II supernovae mainly synthesize oxygen and the  $\alpha$  elements, while Type Ia supernovae produce elements of the iron peak (V, Cr, Mn, Fe, Co and Ni).
- The progenitors of Type II supernovae are massive stars: short time scales, while Type Ia supernovae are due to white dwarfs: long time scales.

Figure 6: Type Ia SNe progenitor structure

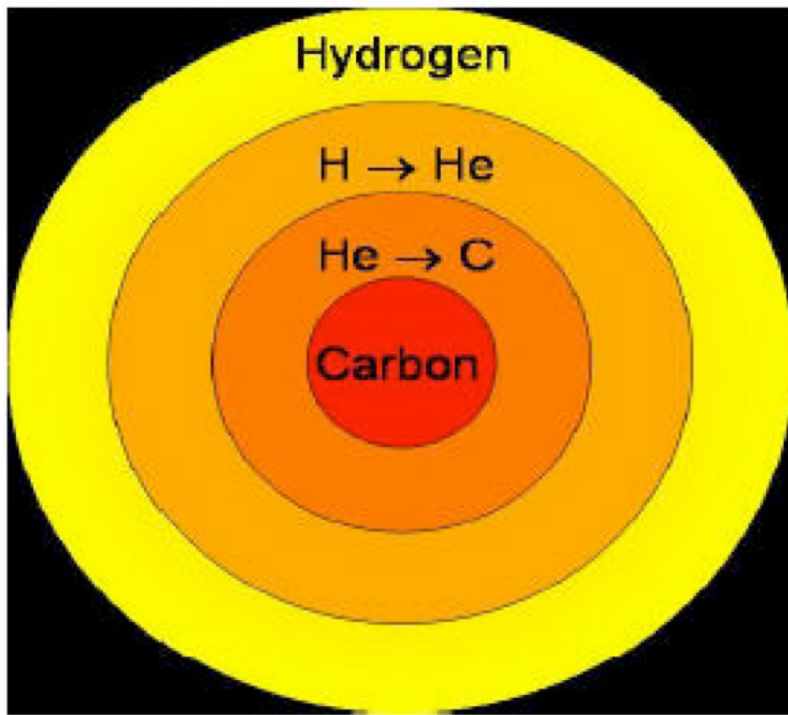
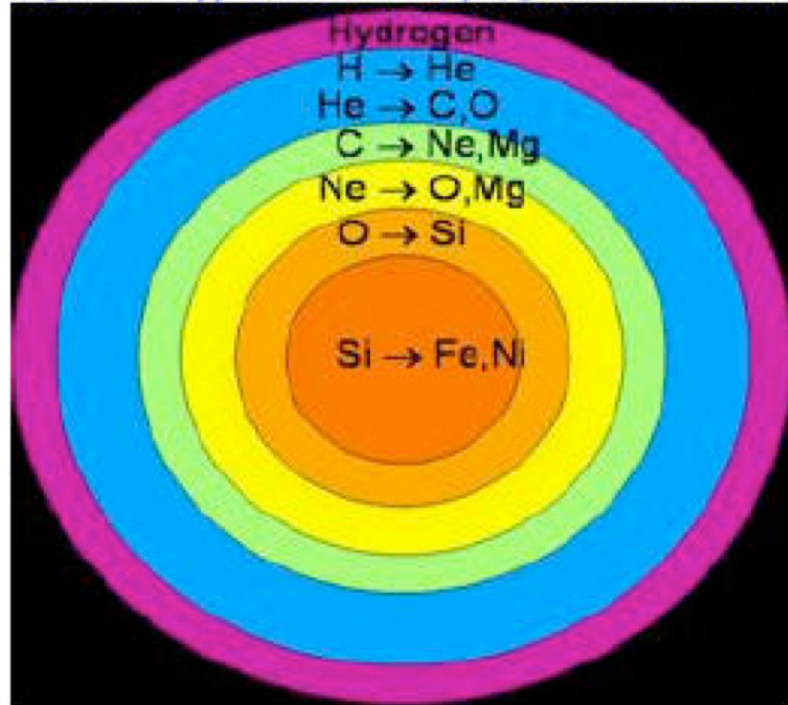


Figure 7: Type Ib, c & II SN progenitor structure



## Chemical yields of SNe

- Type Ia supernovae are due to a white dwarfs in binary systems that accrete mass above the Chandrasekhar mass limit ( $1.4 M_{\odot}$ ) and explode in a runaway fusion reaction (standard candles,  $M_V = -19.3$ , important for cosmology!).
- Type Ia supernovae: long time scales (of the order 1 Gyr after Type II) and net increase of  $[Fe/H]$ , while  $[\alpha/Fe]$  is **decreasing**!
- Type II (core collapse) supernovae: short time scales and net increase of both  $[\alpha/Fe]$  and  $[Fe/H]$ .

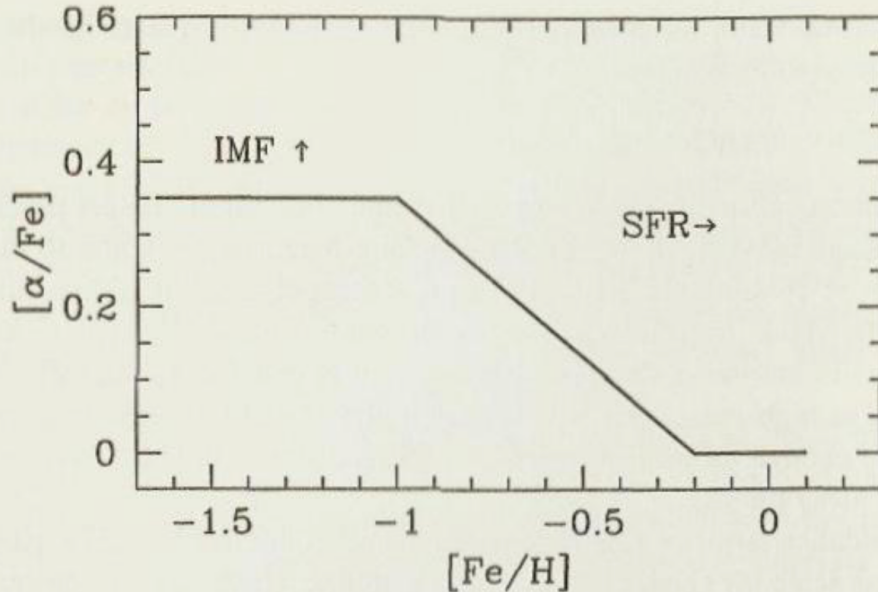
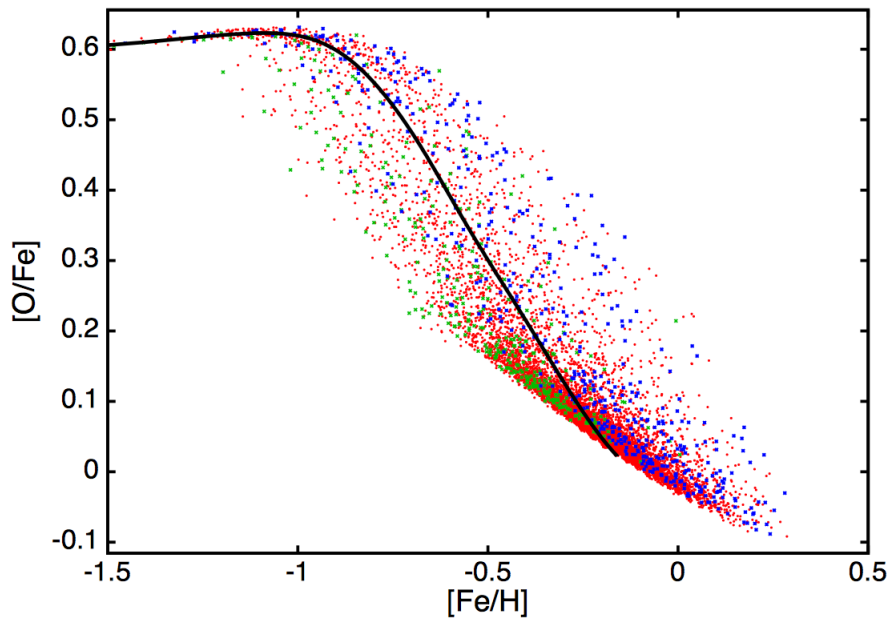


Figure 1 A schematic diagram of the trend of  $\alpha$ -element abundance with metallicity. Increased initial mass function and star formation rate affect the trend in the directions indicated. The knee in the diagram is thought to be due to the onset of type Ia supernovae (SN Ia).

McWilliam  
 (1997, ARA&A 35, 503)

## Generic model prediction for the path through the $[\alpha/Fe]$ vs. $[Fe/H]$ diagram

- A population of stars starts at high  $[O/Fe]$  and low  $[Fe/H]$ , upper left, and moves towards the lower right corner.
- *The curve is parametrized by time, increasing from the top left towards the lower right.*
- Quantitative details depend on star formation rate as a function of time, SN rates and their chemical yields, selection function, etc.

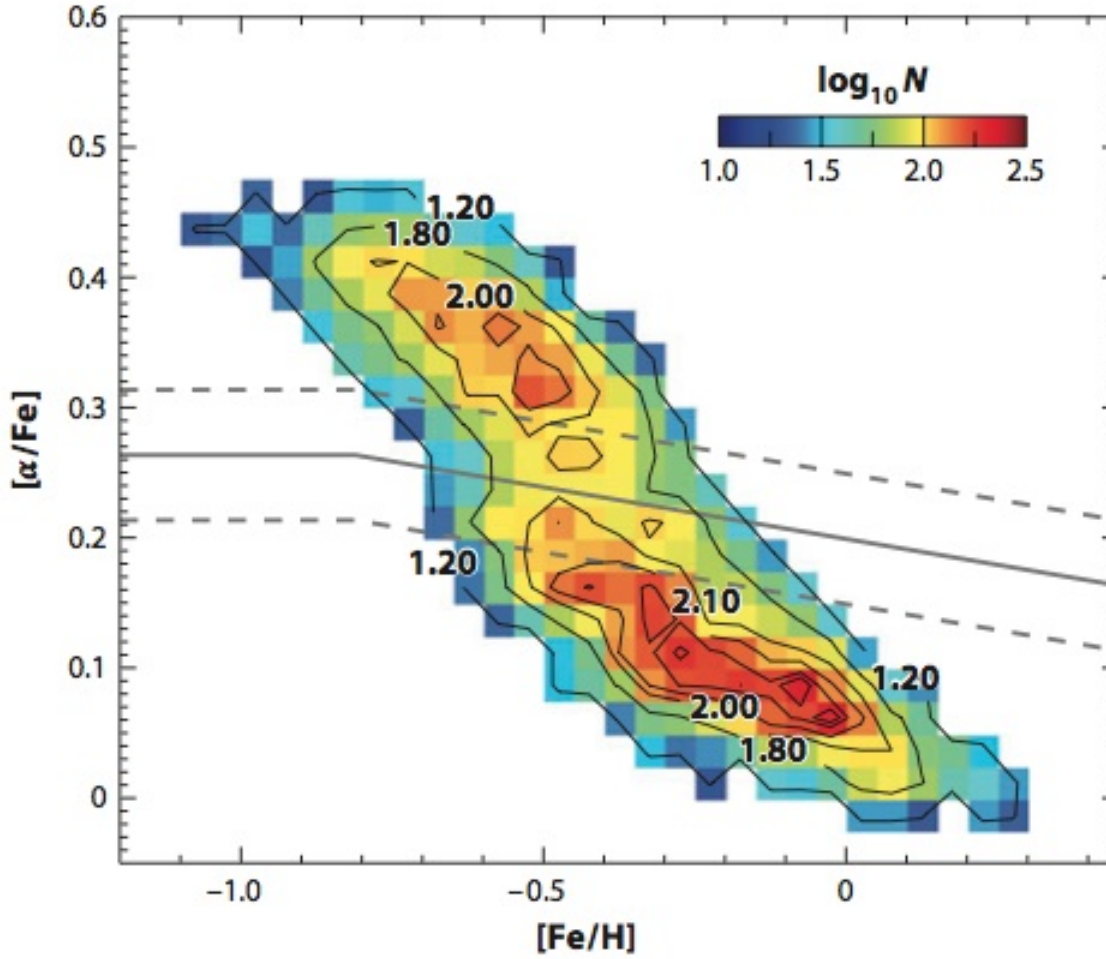


**Figure 9.** The predicted distribution of solar-neighbourhood stars in the  $([\text{Fe}/\text{H}], [\text{O}/\text{Fe}])$  plane. The sample is obtained by using the selection function of the GCS survey as described in

Model-based distribution from Schönrich & Binney (2009, MNRAS 396, 203). It shows the predicted distribution of stars from the solar neighbourhood (with a selection function from the Geneva-Copenhagen survey).

## Generic model prediction for the path through the $[\alpha/\text{Fe}]$ vs. $[\text{Fe}/\text{H}]$ diagram

- A population of stars starts at high  $[\text{O}/\text{Fe}]$  and low  $[\text{Fe}/\text{H}]$ , upper left, and moves towards the lower right corner.
- *The curve is parametrized by time, increasing from the top left towards the lower right.*
- Quantitative details depend on star formation rate as a function of time, SN rates and their chemical yields, selection function, etc.
- Recent progress: is the observed bimodal structure a selection effect or not? (HW 3!)

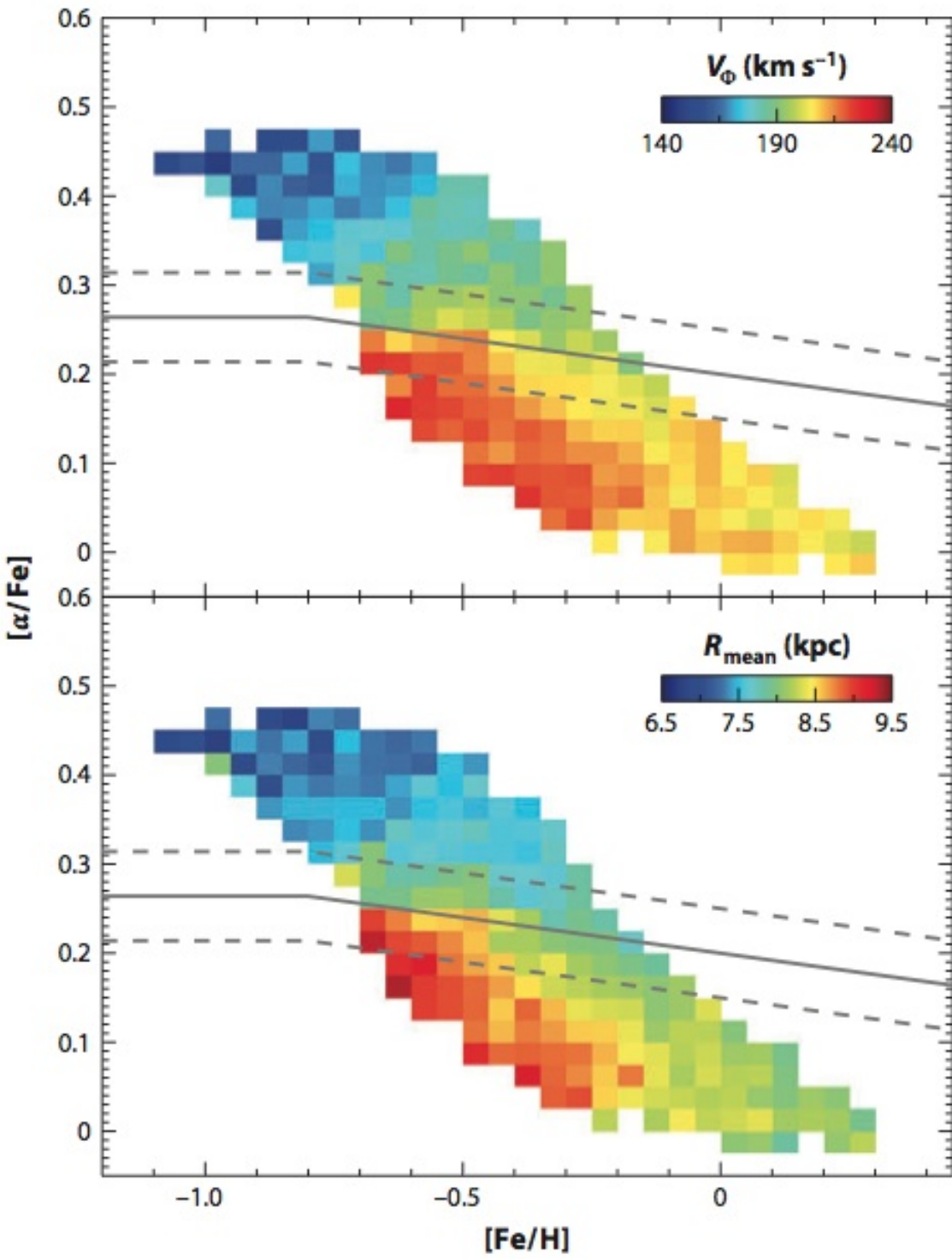


## [ $\alpha$ /Fe] distribution for disk stars

- 17,000 G dwarfs with SDSS [ $\alpha$ /Fe] measurements (Lee et al. 2011).
- **Bimodal distribution!**
- Strongly suggests a thin/thick disk separation based solely on [ $\alpha$ /Fe] (age proxy?)

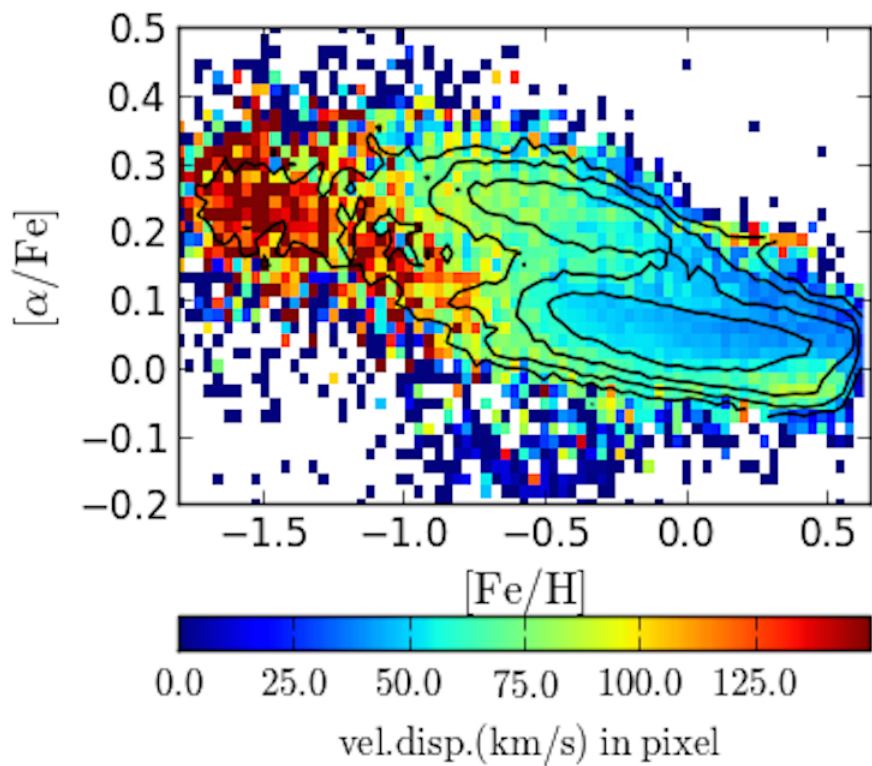
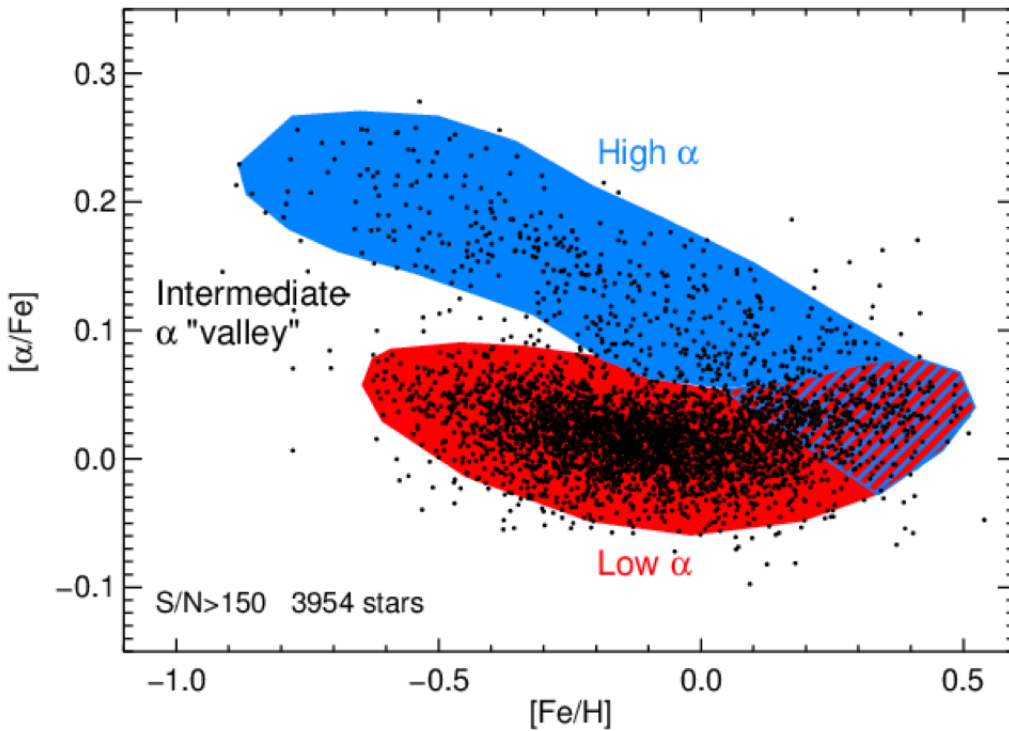
**Figure 8**

The [ $\alpha$ /Fe] versus [Fe/H] distribution of G-type dwarfs within a few kiloparsecs from the Sun. The number density (arbitrarily normalized) is shown on a logarithmic scale according to the legend and by isodensity contours. Each pixel (0.025 dex in the [ $\alpha$ /Fe] direction and 0.05 dex in the [Fe/H] direction) contains at least 20 stars (with a median occupancy of 70 stars). The distribution of disk stars in this diagram can be described by two components (thin disk and thick disk, respectively) centered on ( $[Fe/H]$ ,  $[\alpha/Fe]$ ) = ( $-0.2, +0.10$ ) and ( $-0.6, +0.35$ ). The solid gray line is the fiducial for division into likely thin- and thick-disk populations; note that a simple  $[\alpha/Fe] = 0.24$  separation results in almost identical subsamples. The dashed gray lines show the selection boundaries adopted by Lee et al. (2011b), which exclude the central overlap region. Adapted from Lee et al. (2011b).



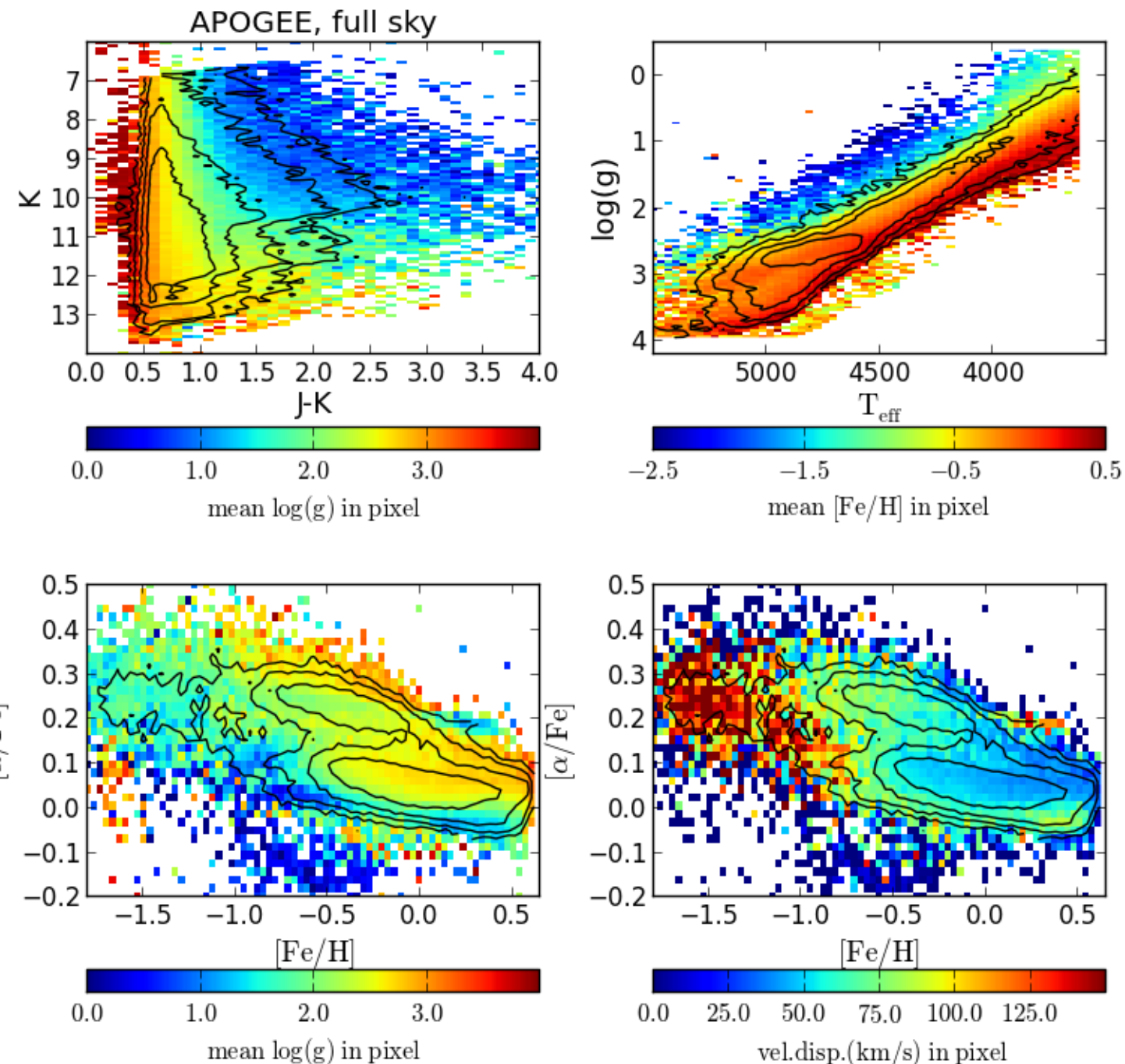
## $[\alpha/Fe]$ distribution for disk stars

- Strong correlation of orbital parameters (top: rotational velocity; bottom: mean orbital radius) with the position in the  $[\alpha/Fe]$  vs.  $[Fe/H]$  plane.
- Bovy, Rix & Hogg (2012) claim(ed) a continuous behavior rather than a two-component decomposition.
- The differences in  $[\alpha/Fe]$  likely reflect different star-formation timescales (enrichment by Type Ia versus Type II supernovae for low and high  $[\alpha/Fe]$  values over long and short timescales, respectively), see Bensby et al. (2004).

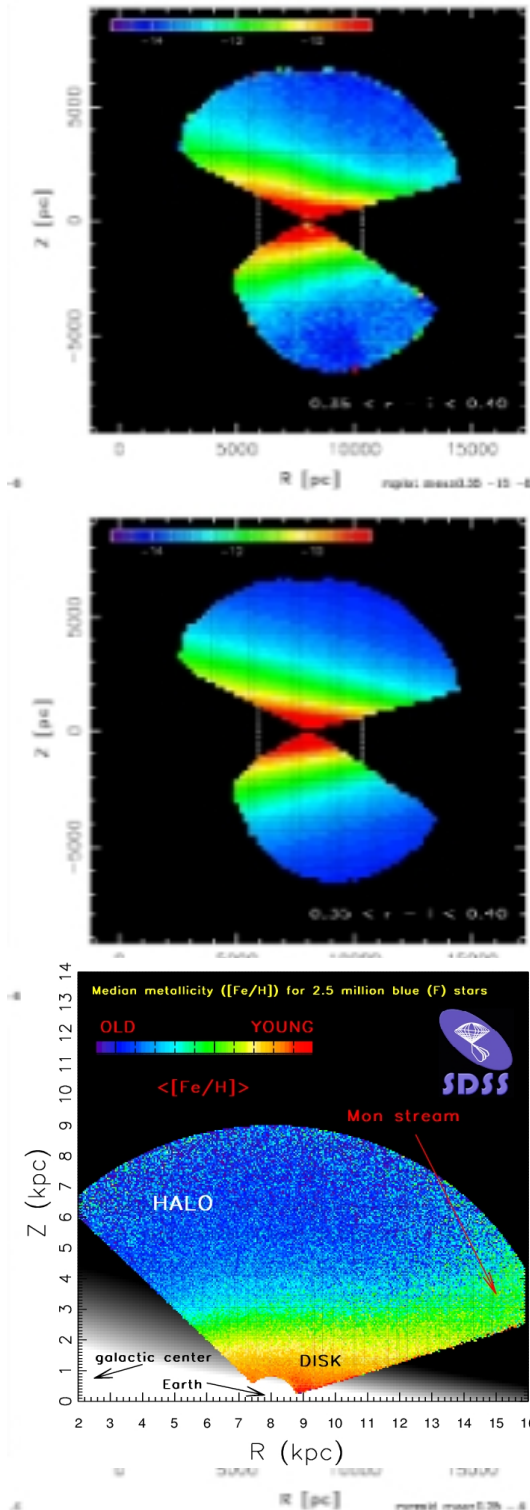


## [ $\alpha$ /Fe] distribution for disk stars

- Latest news from Nidever, Bovy et al. (2014, ApJ 796, 38): “The clear [ $\alpha$ /Fe] bimodality in the APOGEE data . . . and we confirm this result . . . and find that it is not caused by selection effects.”
- With APOGEE measurements (SDSS Data Release 12, bottom left), the observed bimodality is self-evident. Also, note contamination by halo stars at  $[Fe/H] < -1$ , easily recognized from elevated velocity dispersion. Btw, this sounds so like HW3...

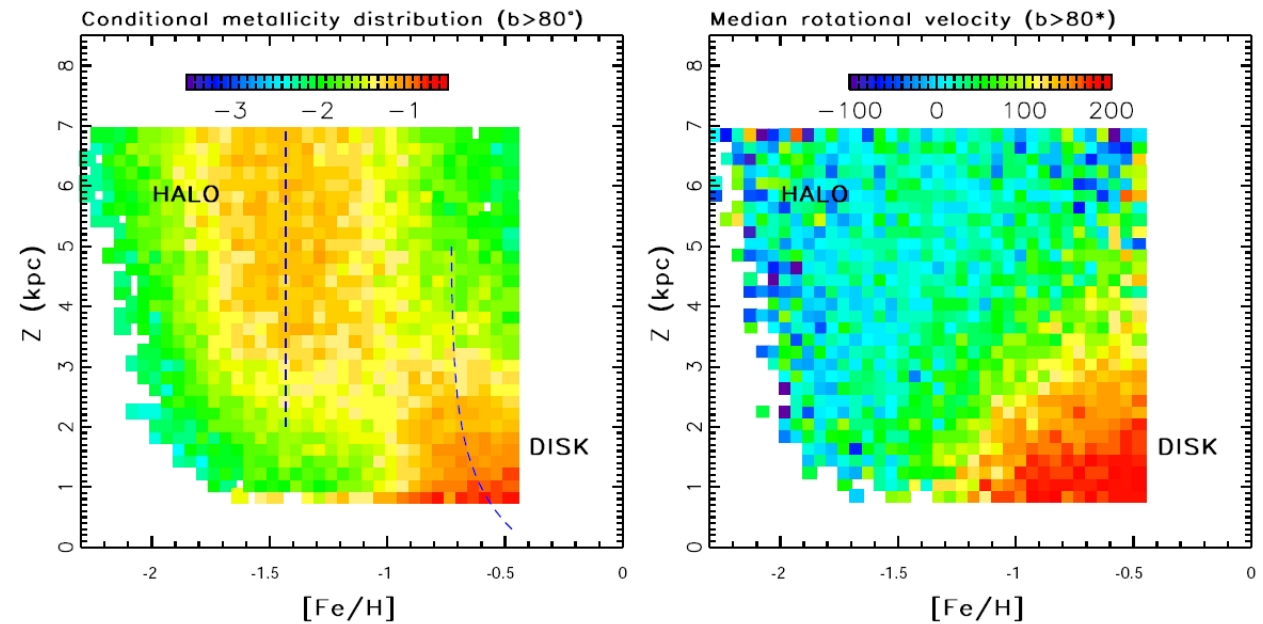


$0.35 < r-i < 0.40$

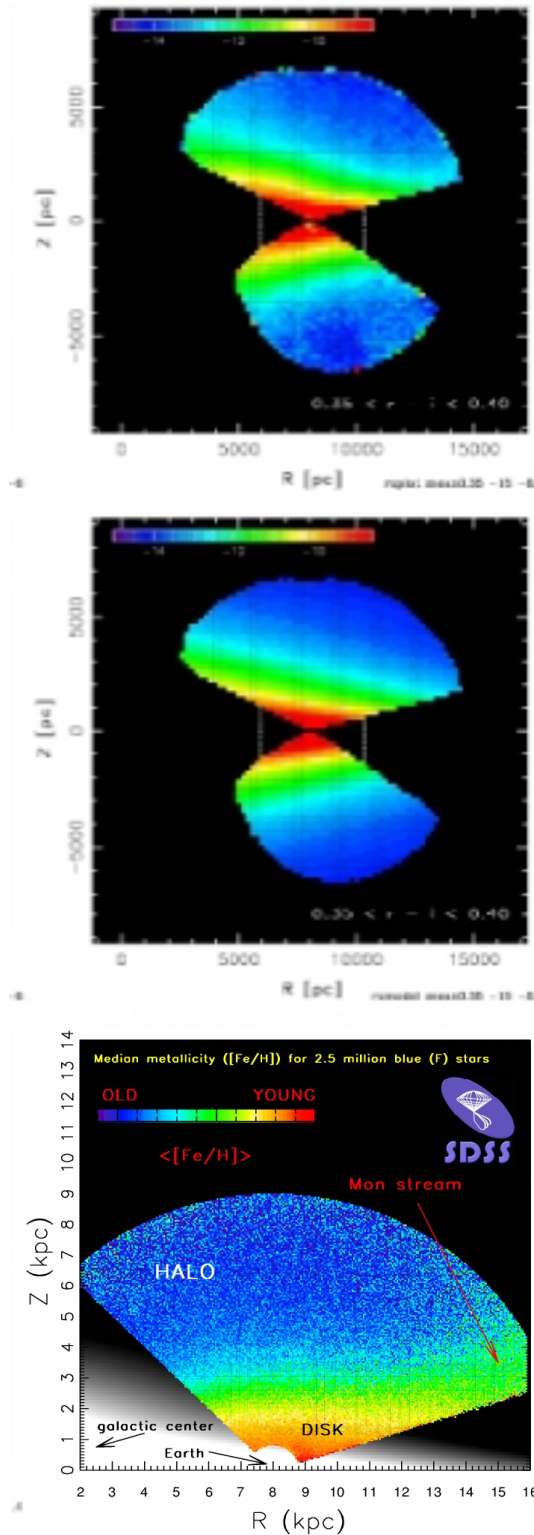


## Dissecting the Milky Way with SDSS

- Panoramic view of the Milky Way, akin to observations of external galaxies; good support for standard Galactic models (with amazing signal-to-noise!)
- Metallicity mapping supports components inferred from number counts mapping
- Kinematics are correlated with metallicity
- Kinematics provide constraints on gravitational potential and initial conditions

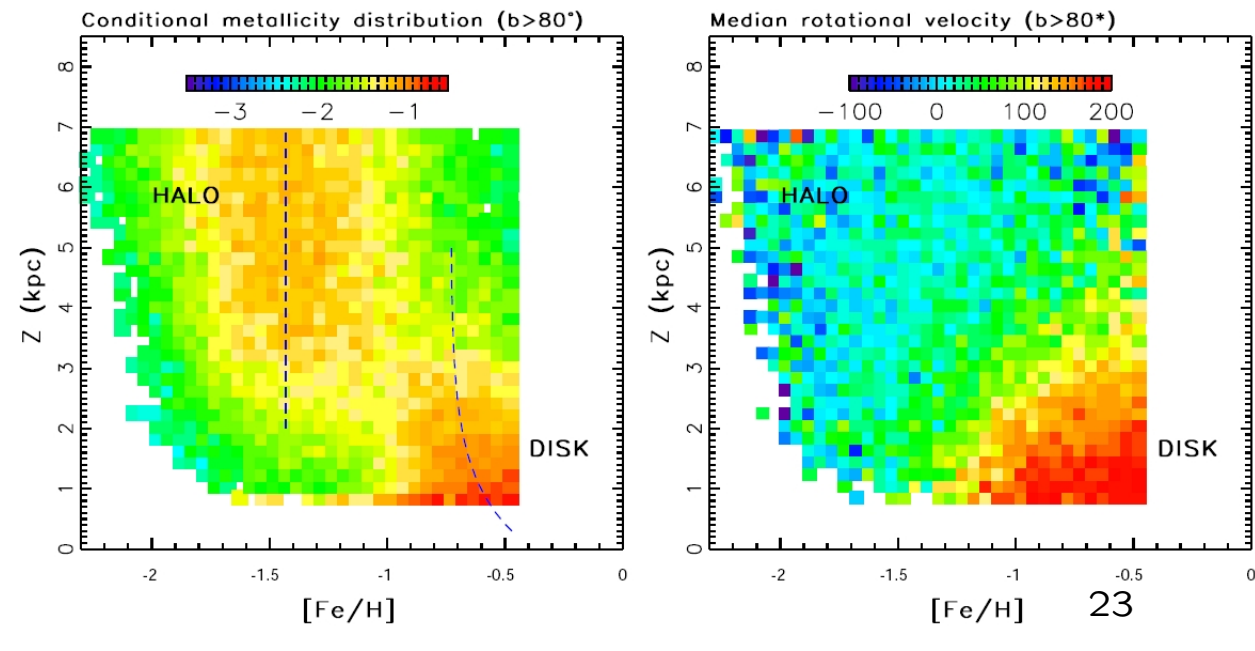


$0.35 < r-i < 0.40$



## Dissecting the Milky Way with SDSS

- Kinematics present a much harder analysis problem than counts and  $[Fe/H]$ ; instead of a single count value, or a scalar distribution function, at each position we need to study a 3-dimensional distribution function  $p(v_\phi, v_R, v_Z)$ !
- Need to measure velocities! (Lecture 5)
- (we can't measure acceleration – except in special cases, such as orbits of stars in the Galactic center as we already discussed)



# Velocity measurements

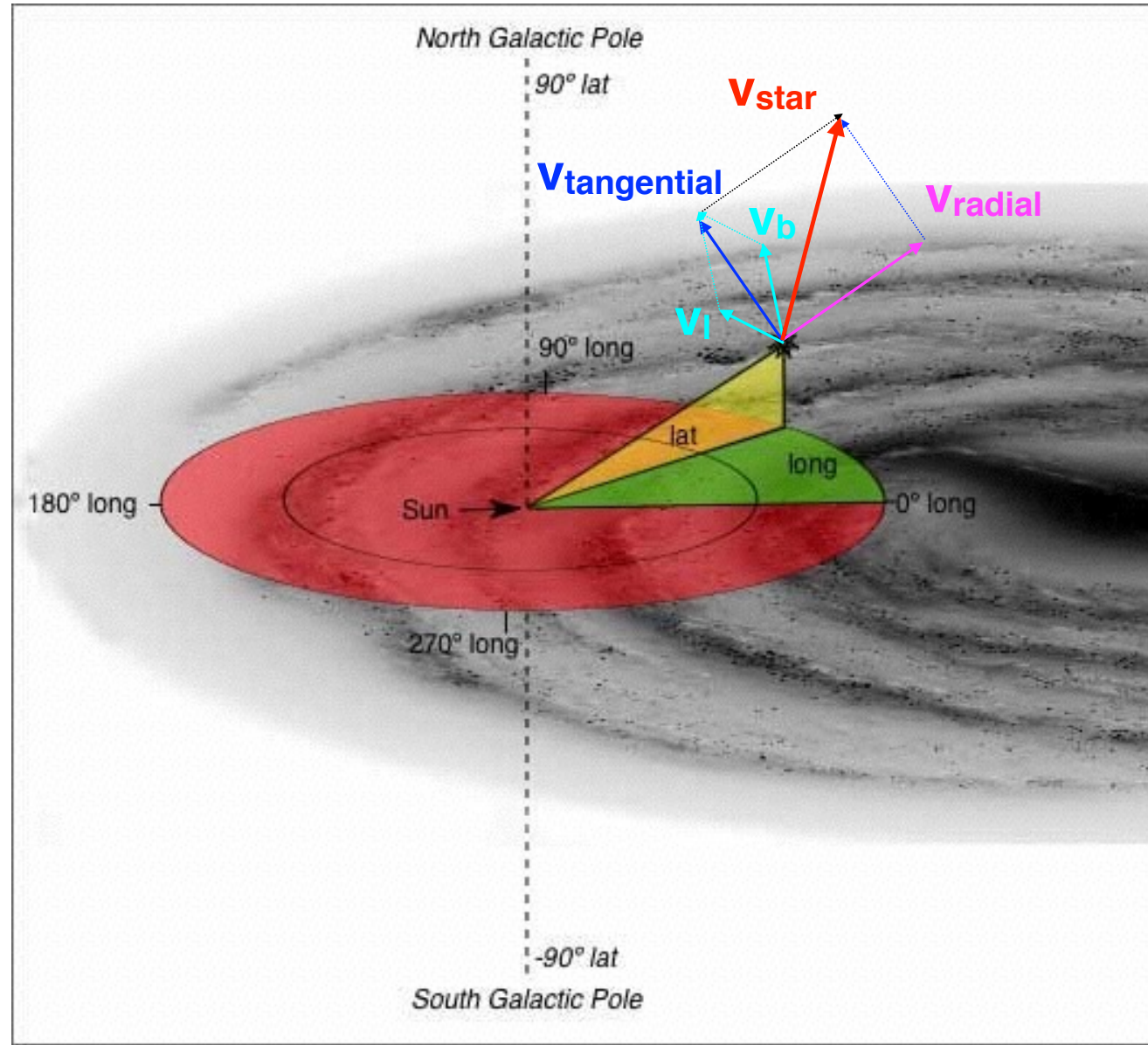
- Velocity can be expressed as a (vector) sum of the component along the line of sight, or radial velocity ( $v_{rad}$ ), and the component perpendicular to the line of sight, or tangential velocity ( $v_{tan}$ ).
- Radial velocity is measured from spectra; large modern stellar spectroscopic surveys, such as SDSS and RAVE, obtain errors of a few km/s (a revolution: close to  $10^6$  spectra!)
- Tangential velocity is measured from proper motion: angular displacement of stars on the sky (typically a tiny fraction of an arcsecond per year, but the record holder, Barnard's star, moves at 10 arcsec/yr); the two best large proper motion catalogs are based on the Hipparcos survey (an astrometric satellite, accuracy of  $\sim$ milliarcsec/yr for  $V < 10$ ), and the SDSS-POSS catalog ( $5 \times 10^7$  stars, 3-5 mas/yr to  $V < 20$ )

## Velocity measurements

- To get tangential velocity,  $v$ , from proper motion,  $\mu$ , distance  $D$  must be known:

$$v = 4.74 \frac{\mu}{\text{mas/yr}} \frac{D}{\text{kpc}} \quad \text{km/s} \quad (1)$$

- At a distance of 1 kpc, and for proper motions good to  $\sim$ mas/yr, the tangential velocity errors are similar to radial velocity errors from SDSS and RAVE
- The advantage of radial velocity is that its measurement does not require distance, while the advantage of proper motion measurements is that they are much “cheaper”



# Velocity measurements

- Assume that  $v_{rad}$  and the two components of tangential velocity,  $v_l$  (in the direction of the galactic longitude) and  $v_b$  (in the direction of the galactic latitude), are known.
- The Cartesian velocity components can be computed from

$$v_X^{obs} = -v_{rad} \cos(l) \cos(b) + v_b \cos(l) \sin(b) + v_l \sin(l)$$

$$v_Y^{obs} = -v_{rad} \sin(l) \cos(b) + v_b \sin(l) \sin(b) - v_l \cos(l)$$

$$v_Z^{obs} = -v_{rad} \sin(b) + v_b \cos(b)$$

- For completeness (right-handed coordinate system!):

$$X = R_\odot - D \cos(l) \cos(b)$$

$$Y = -D \sin(l) \cos(b)$$

$$Z = D \sin(b)$$

## Velocity measurements

- Assume that  $v_{rad}$  and the two components of tangential velocity,  $v_l$  (in the direction of the galactic longitude) and  $v_b$  (in the direction of the galactic latitude), are known.
- The Cartesian velocity components can be computed from

$$v_X^{obs} = -v_{rad} \cos(l) \cos(b) + v_b \cos(l) \sin(b) + v_l \sin(l)$$

$$v_Y^{obs} = -v_{rad} \sin(l) \cos(b) + v_b \sin(l) \sin(b) - v_l \cos(l)$$

$$v_Z^{obs} = -v_{rad} \sin(b) + v_b \cos(b)$$

- Locally, these components are related to more traditional nomenclature as  $v_X = -U$ ,  $v_Y = -V$ , and  $v_Z = W$ .

# Velocity measurements

- How do we go from the measured  $v_X$ ,  $v_Y$ , and  $v_Z$  for a star, to **its own galactocentric**  $v_R$ ,  $v_\phi$ , and  $v_Z$ ?
- First, **we need to account for our motion**. When reporting radial velocity, the projection of Earth's orbital motion (up to 30 km/s!) is typically corrected. Hence, we *only* need to correct for the solar motion around the center of the Milky Way ( $v^\odot$ ):

$$\begin{aligned}v_X^{obs} &= v_X^* + v_X^\odot \\v_Y^{obs} &= v_Y^* + v_Y^\odot \\v_Z^{obs} &= v_Z^* + v_Z^\odot\end{aligned}$$

where  $v^*$  corresponds to a **star's own motion** around the center of the Milky Way (this is what we want to get)

# Velocity measurements

- The solar motion is traditionally decomposed into the **rotational** motion of the Local Standard of Rest and the solar **peculiar** motion:

$$\begin{aligned}v_X^\odot &= v_X^{\odot, pec} \\v_Y^\odot &= -v_{LSR} + v_Y^{\odot, pec} \\v_Z^\odot &= v_Z^{\odot, pec}\end{aligned}$$

- **Note the minus sign in front of  $v_{LSR}$ !** Usually it is assumed that  $v_{LSR} = 220 \text{ km/s}$  (based on HI measurements by Gunn, Knapp & Tremaine 1979), but some recent papers claim that it could be off by as much as 20-30 km/s (some methods are sensitive to uncertain  $R_* = 8.0 \text{ kpc!}$ )

# Velocity measurements

- The solar peculiar motion is obtained by averaging the motions of a large number of stars from the (local) solar neighbourhood (so that their peculiar velocities cancel out)
- Currently the best measurement of the solar peculiar motion is based on Hipparcos data (Dehnen & Binney 1998):  
 $v_X^{\odot,pec} = -10.0 \text{ km/s}$ ,  $v_Y^{\odot,pec} = -5.3 \text{ km/s}$ ,  $v_Z^{\odot,pec} = 7.2 \text{ km/s}$ .
- But recently they revisited this problem (Schönrich, Binney & Dehnen 2010):  
 $v_X^{\odot,pec} = -11.1 \text{ km/s}$ ,  $v_Y^{\odot,pec} = -12.2 \text{ km/s}$ ,  $v_Z^{\odot,pec} = 7.3 \text{ km/s}$
- The measured mean  $Y$  velocity component depends greatly on the selected type of stars (the so-called *asymmetric drift*).

# Velocity measurements

- How do we go from the measured  $v_X$ ,  $v_Y$ , and  $v_Z$  for a star, to **its own galactocentric**  $v_R$ ,  $v_\phi$ , and  $v_Z$ ?
- First, we need to account for our motion:

$$\begin{aligned}v_X^* &= v_X^{obs} - v_X^\odot \\v_Y^* &= v_Y^{obs} - v_Y^\odot \\v_Z^* &= v_Z^{obs} - v_Z^\odot\end{aligned}$$

- After  $(v_X^*, v_Y^*, v_Z^*)$  are known, and assuming that the position of the star,  $(X^*, Y^*, Z^*)$ , is known too, this is simply a coordinate system transformation ( $R = \sqrt{X^2 + Y^2}$ )

$$\begin{aligned}v_R^* &= v_X^* \frac{X^*}{R^*} + v_Y^* \frac{Y^*}{R^*} \\v_\phi^* &= -v_X^* \frac{Y^*}{R^*} + v_Y^* \frac{X^*}{R^*}\end{aligned}$$

## Oort's constants

If we have kinematic measurements for nearby stars at a range of Galactic longitudes ( $l$ ),

$$\frac{v_{rad}^{obs}(l)}{D} = A \sin(2l) \quad (2)$$

$$\frac{v_{tan}^{obs}(l)}{D} = A \cos(2l) + B \quad (3)$$

where  $D$  is star's distance and **Oort's constants**  $A$  and  $B$  are defined as

$$A \equiv \frac{1}{2} \left( \frac{v_c}{R} - \frac{dv_c}{dR} \right)_{R_\odot} \quad (4)$$

$$B \equiv -\frac{1}{2} \left( \frac{v_c}{R} + \frac{dv_c}{dR} \right)_{R_\odot}, \quad (5)$$

we can estimate  $v_c(R_\odot)$  and the  $dv_c/dR$  derivative at  $R = R_\odot$ .

Note from eq. 3 that  $A$  and  $B$  can be estimated from proper motions only, i.e. **without** radial velocities.

## Oort's constants

In the solar neighborhood,

$$A = 14.5 \pm 1.5 \text{ km/s/kpc}, \quad B = -12 \pm 3 \text{ km/s/kpc}. \quad (6)$$

N.B. implied proper motions for a star at 1 kpc are up to  $\sim 5$  mas/yr.

Since the difference  $A - B$  is not vanishing, locally the radial velocity curve is not flat. However, note that  $A - B$  is consistent with zero to within quoted uncertainties!

For improvements to this “epicycle” approximation see Dehnen 1999 (AJ 118, 1190).

# Velocity Distribution Function

- Given  $(v_R^*, v_\phi^*, v_Z^*)$  measurements, how do we analyze them? (hereafter, droping superscript \*)
- For a given control volume,  $dV$ , positioned at  $(X, Y, Z)$ , and using an appropriately chosen subsample of stars described by *tags* (e.g.  $[Fe/H]$ ,  $M_r$ , mass, age), we can define a multi-dimensional distribution function,  $p(v_R, v_\phi, v_Z, X, Y, Z, \text{tags})$ , such that the number of stars,  $dN$ , in that (spatial) volume with velocities in the range  $v_i$  to  $v_i + dv_i$ , with  $i = R, \phi, Z$ , is

$$dN(X, Y, Z, v_R, v_\phi, v_Z, \text{tags}) = \\ p(v_R, v_\phi, v_Z, X, Y, Z, \text{tags}) dV dv_R dv_\phi dv_Z$$

# Velocity Distribution Function

- The normalization of this (complex!) function depends on the **spatial variation of density profiles** which we already studied, metallicity distribution, and the **luminosity function** for each Galaxy component (e.g. disk and halo, which in principle also depend on position). Assuming only three tags ( $M_r$ ,  $[Fe/H]$ , age), we can formally write (| means “given”)

$$\begin{aligned} p(v_R, v_\phi, v_Z, X, Y, Z, M_r, [Fe/H], \text{age}) = \\ f(v_R, v_\phi, v_Z | X, Y, Z, M_r, [Fe/H], \text{age}) \\ \times \rho(X, Y, Z | M_r, [Fe/H], \text{age}) \\ \times \Phi(M_r | [Fe/H], \text{age}) \times p([Fe/H] | \text{age}) \times p(\text{age}) \end{aligned}$$

- Here, we would like to measure and understand theoretically the **shape** of  $f(v_R, v_\phi, v_Z | X, Y, Z, \text{tags})$  (leaving normalization aside for now), and how it varies with  $(X, Y, Z)$  and as a function of various *tags*.

# Velocity Distribution Function

- Traditionally, the measurements were confined to the solar neighborhood (e.g. practically all Hipparcos stars are closer than 100 pc); hence, we knew little about the spatial variation of  $f(v_R, v_\phi, v_Z | X, Y, Z, \text{tags})$ . Also, there are very few halo stars (< 1%) in local samples, so the variation as a function of metallicity was not well measured either.
- Local measurements of smallish samples were consistent with a 3-dimensional gaussian distribution: **the Schwarzschild velocity ellipsoid**

$$f(v_R, v_\phi, v_Z) = \prod_{i=1}^3 G(\bar{v}_i, \sigma_i)$$

where  $\bar{v}_i$  are *mean velocities*, and  $\sigma_i$  are *velocity dispersions* in the principal directions. In a special case when the velocity ellipsoid is aligned with the coordinate system, the principal directions are the coordinate axes.

# Velocity Distribution Function

Within the paradigm of **velocity ellipsoid**, some questions to ask are:

1. Is this gaussian approximation supported by the data? E.g. are there localized cold streams? Multiple gaussian components (disk vs. halo, thin vs. thick disk)?
2. What are the values of  $\bar{v}_i$  and  $\sigma_i$ , and do they depend on position and tags such as metallicity and age?
3. What is the orientation of the velocity ellipsoid?
4. Can we interpret velocity ellipsoid with some “reasonable” gravitational potentials?

We will discuss here some of recent progress enabled by SDSS data (e.g., Bond et al. 2010, ApJ 716, 1)

## SDSS-POSS proper motion measurements

---

- The Munn et al. (2004 AJ, 127, 3034) catalog
  - recalibrated POSS astrometry using galaxies
  - 100,000 quasars (360 per Schmidt plate) for quality assessment: random errors 3 mas/yr (per coordinate) to  $r < 18$ , increases to 6 mas/yr at  $r = 20$ , systematic errors  $\sim 0.3$  mas/yr
  - publicly available as part of SDSS Data Release 6
  - Over 30,000,000, mostly main sequence, stars: the largest accurate proper motion catalog (until Gaia and LSST)

# Independent Test of Systematic Errors

- There are lots of quasars in SDSS-POSS sample, and quasars don't move as fast as  $\sim$ mas/yr.

4

BOND ET AL.

Vol. 716

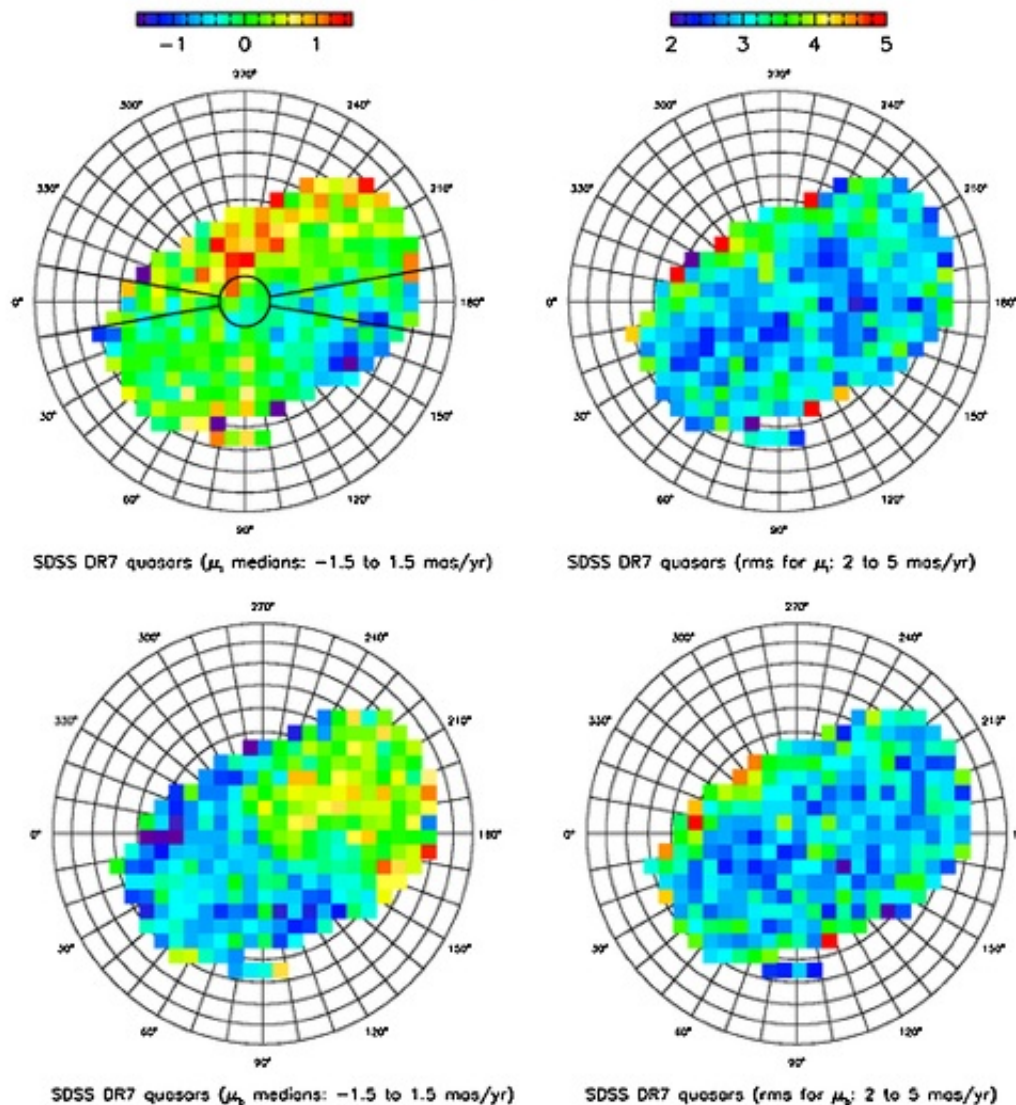
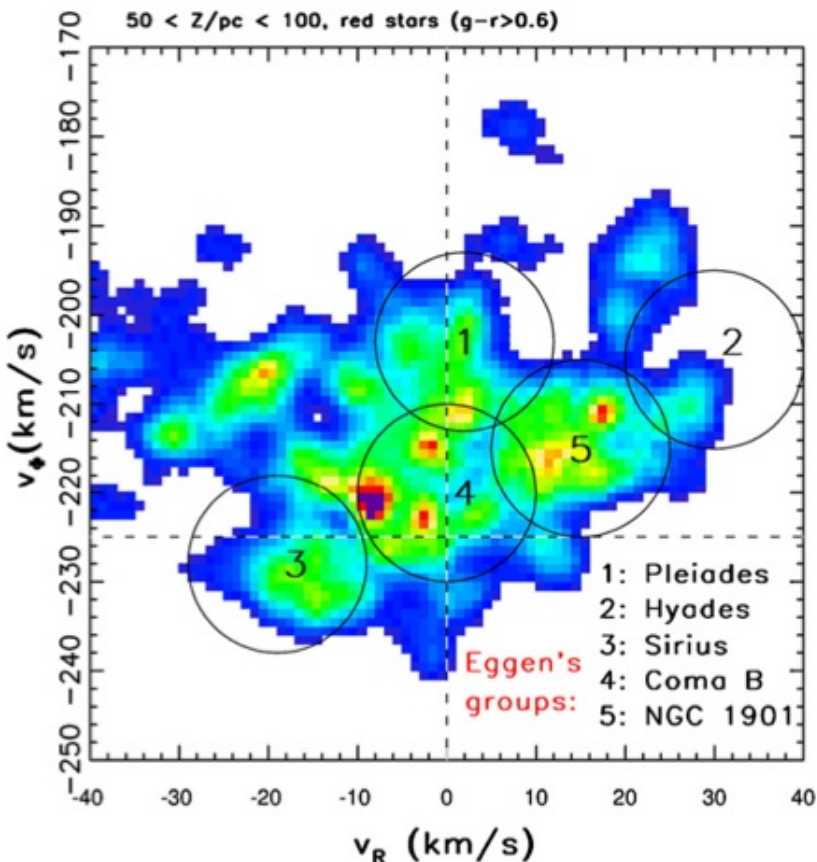
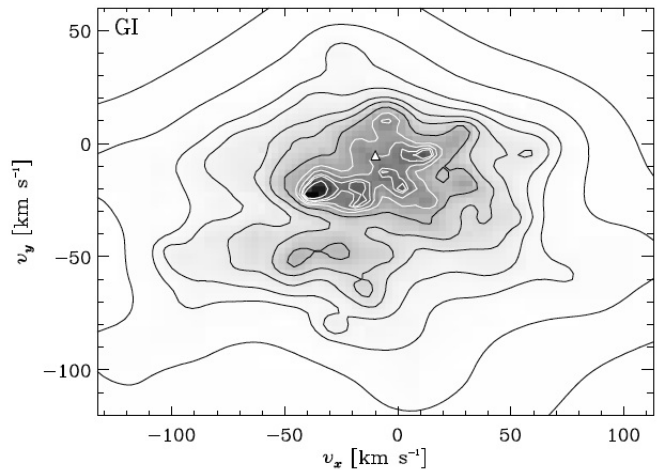


Figure 1. Behavior of proper-motion measurements for 60,000 spectroscopically confirmed SDSS quasars with  $b > 0^\circ$ . The color-coded maps (see the legend on top, units are  $\text{mas yr}^{-1}$ ) show the distribution of the median (left) and rms (right) for the longitudinal (top) and latitudinal (bottom) proper-motion components in a Lambert projection of the northern Galactic cap. The median number of quasars per pixel is  $\sim 250$ . For both components, the scatter across the sky is  $0.60 \text{ mas yr}^{-1}$ . The median proper motion for the full quasar sample is  $0.15 \text{ mas yr}^{-1}$  in the longitudinal direction, and  $-0.20 \text{ mas yr}^{-1}$  in the latitudinal direction. The thick line in the top-left panel shows the selection boundary for the "meridional plane" sample.



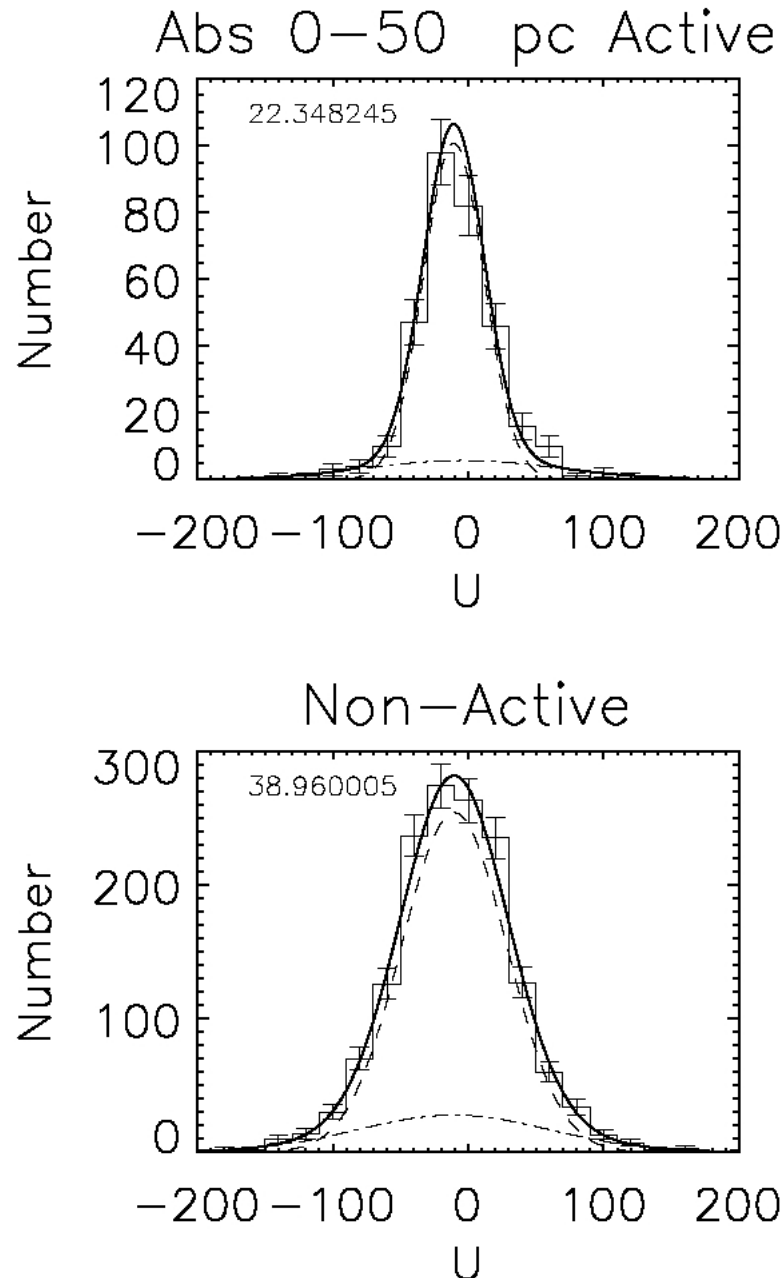
**Figure 4.** Similar to the top-left panel in Figure 3, except that stars are selected from a distance bin that corresponds to *HIPPARCOS* sample ( $Z = 50\text{--}100$  pc). The positions of Eggen's moving groups (Eggen 1996) are marked by circles, according to the legend in the bottom-right corner. The horizontal line at  $v_\phi = -225 \text{ km s}^{-1}$  corresponds to vanishing heliocentric motion in the rotational direction



## Kinematics for nearby stars

- A good summary/definitive analysis of the local Hipparcos sample: Dehnen & Binney (1998, MNRAS 298, 387).
- Within about 100 pc from the plane, the kinematics show a lot of structure: **multiple peaks** (first advocated by Eggen, later demonstrated in Hipparcos data by Dehnen, see bottom left)

## Scattering of Disk Stars



Bochanski et al.  
(2007, AJ 134, 2418)

- Hot blue stars have smaller velocity dispersions than cool red stars; metal-rich stars have smaller velocity dispersions than metal-poor stars
- Active (presumably young) M dwarfs have smaller velocity dispersion than non-active M dwarfs (Bochanski et al. 2007)
- The imperfections in the Galaxy's gravitational field cause the random velocities of stars to increase: **the velocity dispersion increases with age:  $\sigma \propto t^{1/2}$**
- The irregularities responsible for this phenomenon range in scale from small such as **molecular clouds**, to large such as **spiral arms**
- Can we (at least qualitatively) understand this behavior?

## Scattering by molecular clouds

Typical clouds: up to  $10^6 M_\odot$ ,  $< 100$  pc

Spitzer & Schwarzschild (1953) proposed their existence, motivated by the correlation between the velocity dispersion and age, *before* the first ones were detected!

A star has a relative speed with respect to a cloud because of differential rotation. The successive encounters will increase the star's random velocity.

Prediction:  $\sigma \propto t^{1/4}$  slower than observed

Another difficulty: can explain  $\sigma$  of up to 30 km/s, but white dwarfs and C stars have  $\sigma \sim 50$  km/s

## Scattering by spiral arms

N-body simulations: spiral arms can heat the disk

The spiral structure heats the disk, which decreases the efficiency of the swing amplifier until the spiral structure cannot be maintained.

“Thus the spiral structure is killed by the heat that it injects into the disk, just as yeast in a vat of fermenting beer is killed by the alcohol it creates” (from Binney & Tremaine).

Important: a fixed spiral pattern cannot heat the disk – the arms must be transitory (see BT figs. 7-26 and 7-27)

Note that within Lin-Shu theory disk heating is negligible; the stochastic theory predicts significant disk heating

Prediction:  $\sigma \propto t^\alpha$ , with  $\alpha \sim 0.2 - 0.5$  not too bad

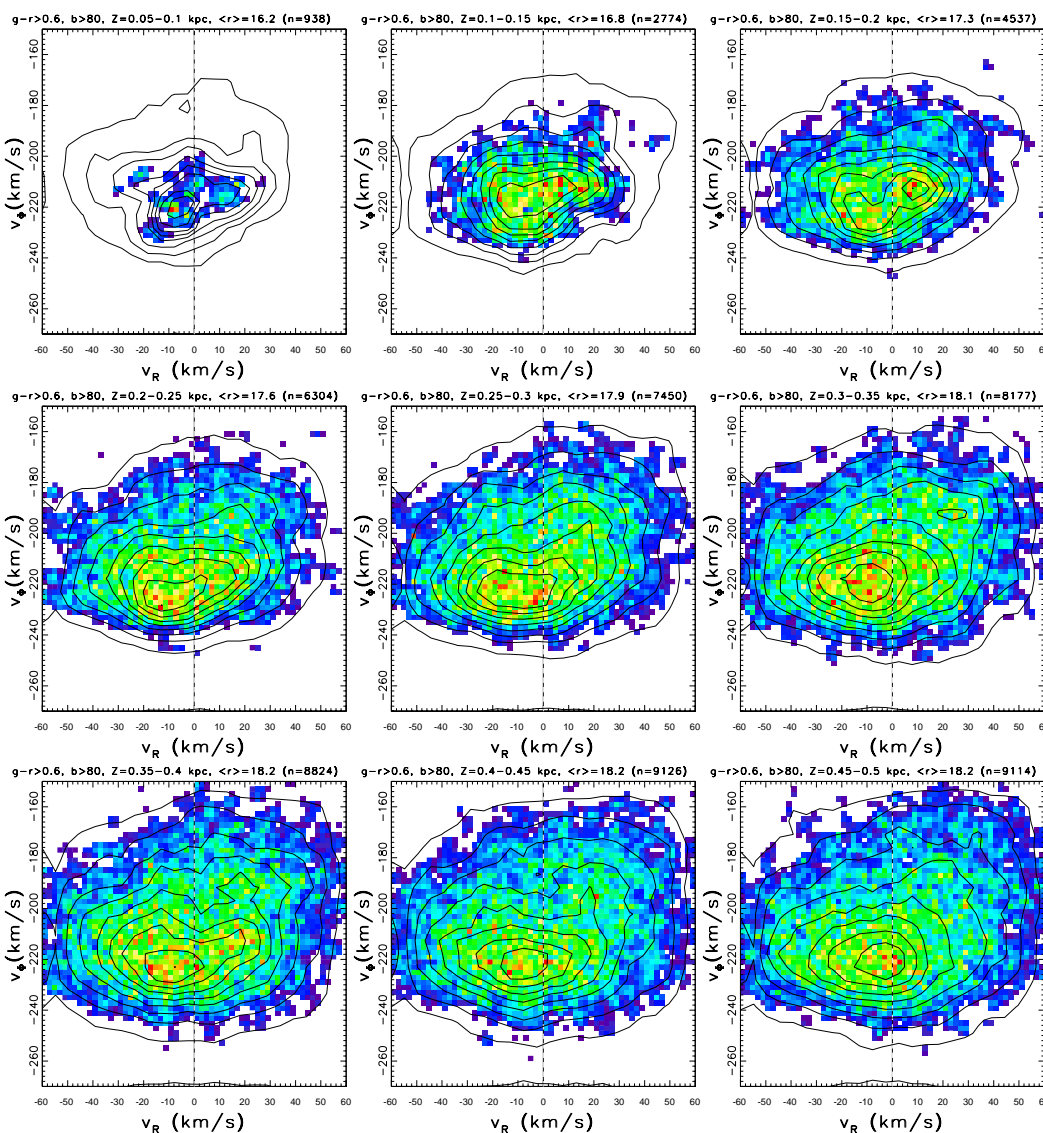
## Scattering by spiral arms

Problem: the velocity dispersion increases only in the radial and azimuthal directions. What about the vertical dispersion?

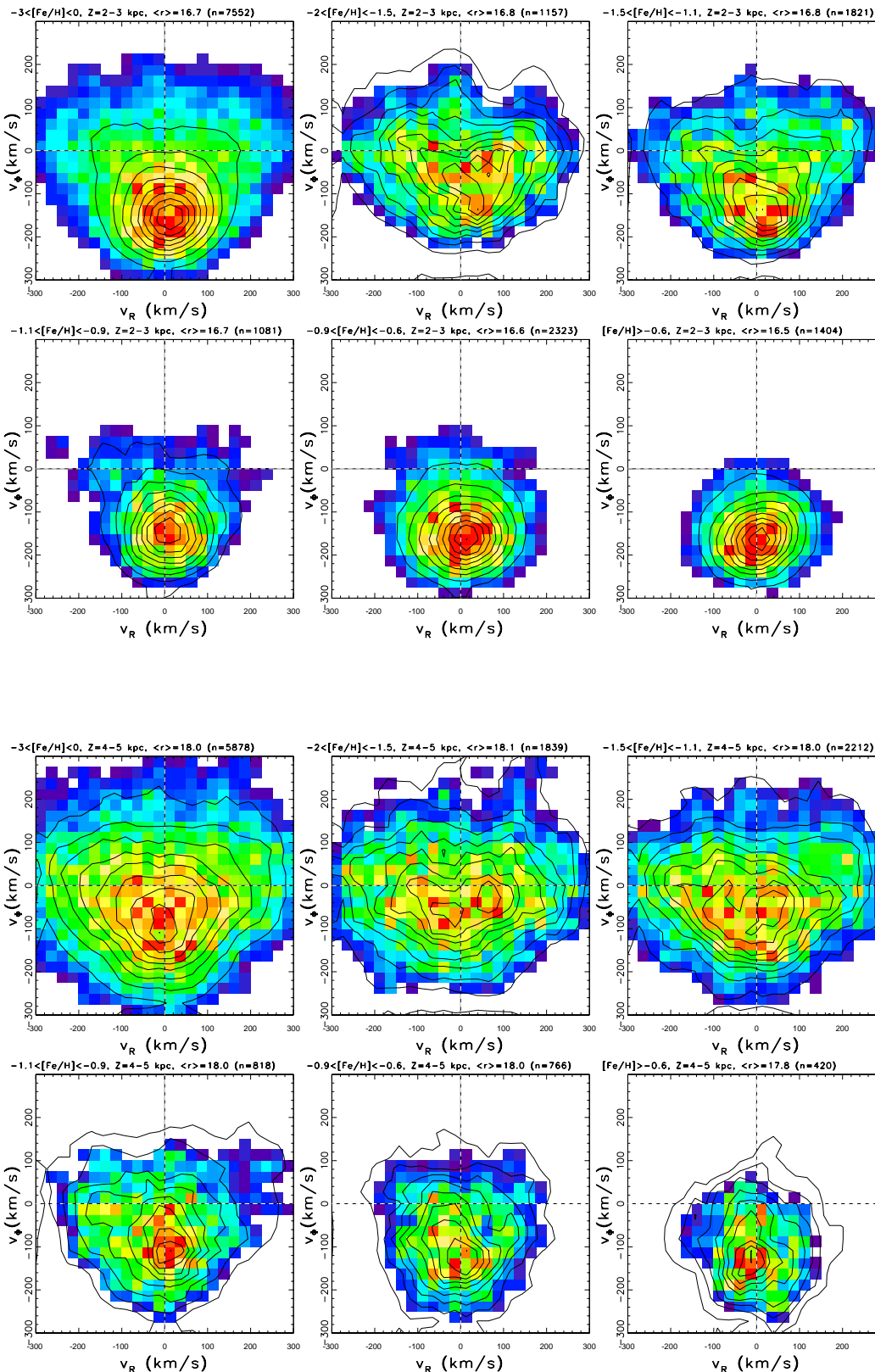
Carlberg (1984): spiral arms provide heating in the radial and azimuthal directions, which molecular clouds redistribute in the vertical direction.

Lacey & Ostriker (1985): the heating is due to  $10^6 M_\odot$  black holes from the halo.

## Kinematics for nearby stars



- Within about 100 pc from the plane, the kinematics show a lot of structure: **multiple peaks** (first advocated by Eggen, later demonstrated in Hipparcos data by Dehnen)
- Panels:**  $f(v_R, v_\phi)$  for red (K and M) main-sequence stars towards the north galactic pole; determined using SDSS-POSS proper motions, in nine 50pc thick  $Z$  slices, from 50 pc to 500 pc
- Beyond 100 pc from the plane, the velocity distribution becomes more similar to a gaussian; however, deviations are clearly detected (due to a large number of stars and well-controlled errors)

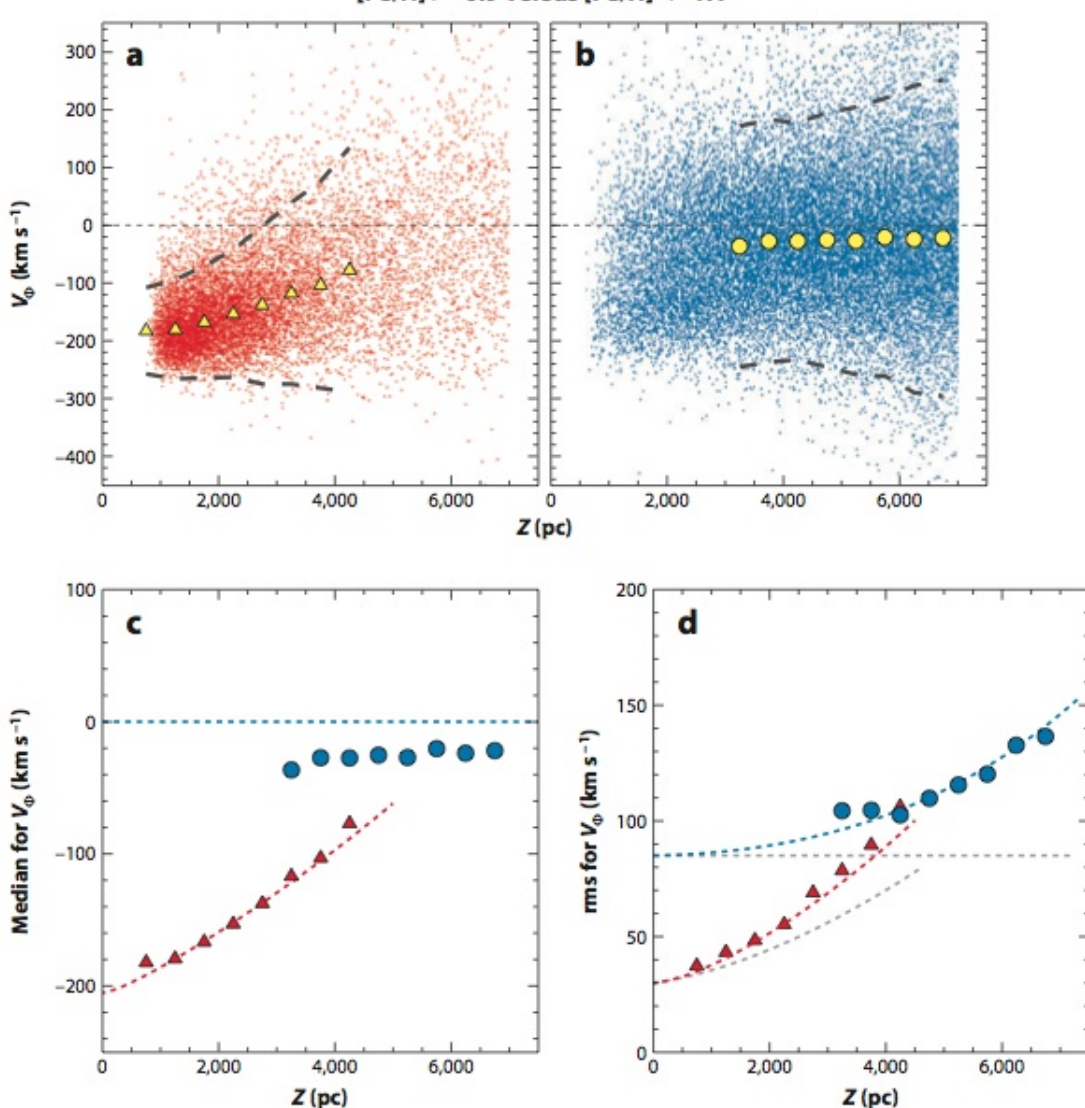


## Kinematics for distant stars

- **Top panels:**  $f(v_R, v_\phi)$  for blue (F and G) main-sequence stars towards the north galactic pole; determined using SDSS-POSS proper motions,  $Z = 2 - 3$  kpc. The top left is the full sample, the other five are for  $[Fe/H]$  slices, from  $-2$  to  $> -0.6$  (halo, halo, mixed, disk, disk)
- **Bottom panels:** analogous, for  $Z = 4 - 5$  kpc.
- **Conclusion:** High-metallicity stars have net rotation (the median velocity depends on  $Z$ ), low-metallicity stars are consistent with no rotation.

## Disk vs. Halo Kinematics

- **Top panels:** small dots are individual stars, large symbols are the median values.
- **Top left:** disk stars show clear velocity shear (increase of  $v_\phi$  with  $Z$ )
- **Top right:** halo stars  $< v_\phi > \sim 220$  km/s
- **Bottom left:** velocity shear is **not** linear
- **Bottom right:** velocity dispersion slowly increases with  $Z$  for disk stars, while for halo stars it is spatially invariant



**Is velocity shear simply a consequence of thick disk becoming dominant over thin disk beyond 1-2 kpc?**

# Is velocity shear simply a consequence of thick disk becoming dominant over thin disk beyond 1-2 kpc?

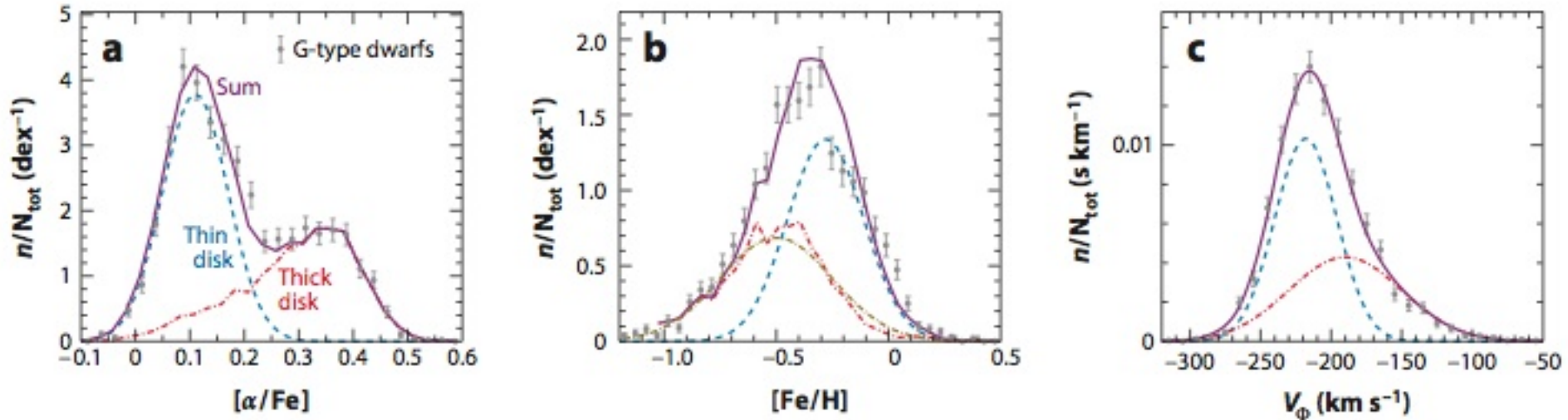


**Figure 12**

Tests of thin-/thick-disk decomposition using the sample of G-type dwarfs from Lee et al. (2011b). (a) The  $[\alpha/\text{Fe}]$  distribution for  $\sim 2,300$  stars in the fiducial bin  $|Z| = 400\text{--}600$  pc as gray circle symbols with (Poissonian) error bars. The bimodality is easily seen. The observed distribution can be modeled as the sum (shown by the *purple solid line*) of two components: the  $[\alpha/\text{Fe}]$  distribution for  $\sim 3,300$  stars with  $|Z| = 2\text{--}3$  kpc shifted to lower values by 0.03 dex (*red dot-dashed line*) and a Gaussian distribution,  $N(0.11, 0.06)$  (*blue dashed line*). The weights for the two components (0.43 and 0.57 for the thick and thin components, respectively) are consistent with a double-exponential fit to star counts. (b) The  $[\text{Fe}/\text{H}]$  distribution for the same stars from the fiducial  $Z = 400\text{--}600$  pc bin as symbols with error bars. Similar to the  $[\alpha/\text{Fe}]$  distribution, it can be modeled as the sum (purple solid line) of two components: the  $[\text{Fe}/\text{H}]$  distribution for stars with  $|Z| = 2\text{--}3$  kpc shifted to higher values by 0.2 dex (*jagged red dot-dashed line*) and  $N(-0.28, 0.17)$  (*blue dashed line*). The weights for the two components (0.43 and 0.57) are the same as in panel a. The  $[\text{Fe}/\text{H}]$  distribution for stars with  $|Z| = 2\text{--}3$  kpc is well described by  $N(-0.50, 0.25)$  (after application of a 0.2 dex offset), shown as the smooth dark yellow dot-dashed line. (c) The rotational velocity distribution for the same stars from the fiducial  $|Z| = 400\text{--}600$  pc bin as symbols with error bars. It can be modeled as a linear combination of two Gaussian distributions,  $N(-218, 22)$  and  $N(-190, 40)$ , again using the same relative weights (and line styles) as in panel a.

## The Local Mass Density

The  $v_z$  Jeans equation (steady-state), see Lecture 7:

$$\frac{\partial(\nu \bar{v}_R v_z)}{\partial R} + \frac{\partial(\nu \bar{v}_z^2)}{\partial z} + \frac{\nu \bar{v}_R v_z}{R} + \nu \frac{\partial \Phi}{\partial z} = 0.$$

Drop the first and third terms because they are a factor of  $\approx z^2/(RR_d)$  smaller than the second and fourth terms:

$$\frac{1}{\nu} \frac{\partial(\nu \bar{v}_z^2)}{\partial z} = - \frac{\partial \Phi}{\partial z} \quad (7)$$

Near the plane of a highly flattened system, Poisson's equation becomes

$$\frac{\partial^2 \Phi}{\partial z^2} = 4\pi G \rho \quad (8)$$

## The Local Mass Density

$$\frac{\partial}{\partial z} \left[ \frac{1}{\nu} \frac{\partial(\nu \bar{v}_z^2)}{\partial z} \right] = -4\pi G \rho \quad (9)$$

If we can measure stellar counts ( $\nu$ ) and velocity dispersion ( $\bar{v}_z^2$ ) (as functions of  $z$ ), then we can determine the local mass density  $\rho$ , which also includes the *dark matter* component, if any. This  $\rho$  is called the Oort limit.

Oort (1932) estimated  $\rho(R_\odot, z = 0) = 0.15 \text{ M}_\odot/\text{pc}^3$ .

Bahcall (1984) estimated  $\rho(R_\odot, z = 0) = 0.18 \pm 0.03 \text{ M}_\odot/\text{pc}^3$ . This appeared as a significant result because the local density of the luminous matter (stars, gas and white dwarfs) is independently estimated at  $0.11 \text{ M}_\odot/\text{pc}^3$ , and thus suggests the existence of dark matter in the disk (the halo dark matter contribution to local  $\rho$  is less than  $0.01 \text{ M}_\odot/\text{pc}^3$ ).

However, Kuijken & Gilmore (1989, MNRAS 239, 651) showed that previous samples and analysis were flawed: there is no evidence that the dynamical mass density is larger than the local density of the luminous matter – both are around  $0.10 \text{ M}_\odot/\text{pc}^3$ .

Bovy & Tremaine (2012, ApJ 756, 89) estimated local dark matter density as

$$\rho_{DM} = (0.008 \pm 0.003) M_\odot \text{pc}^{-3} \quad (0.3 \pm 0.1 \text{ GeVcm}^{-3}) \quad (10)$$

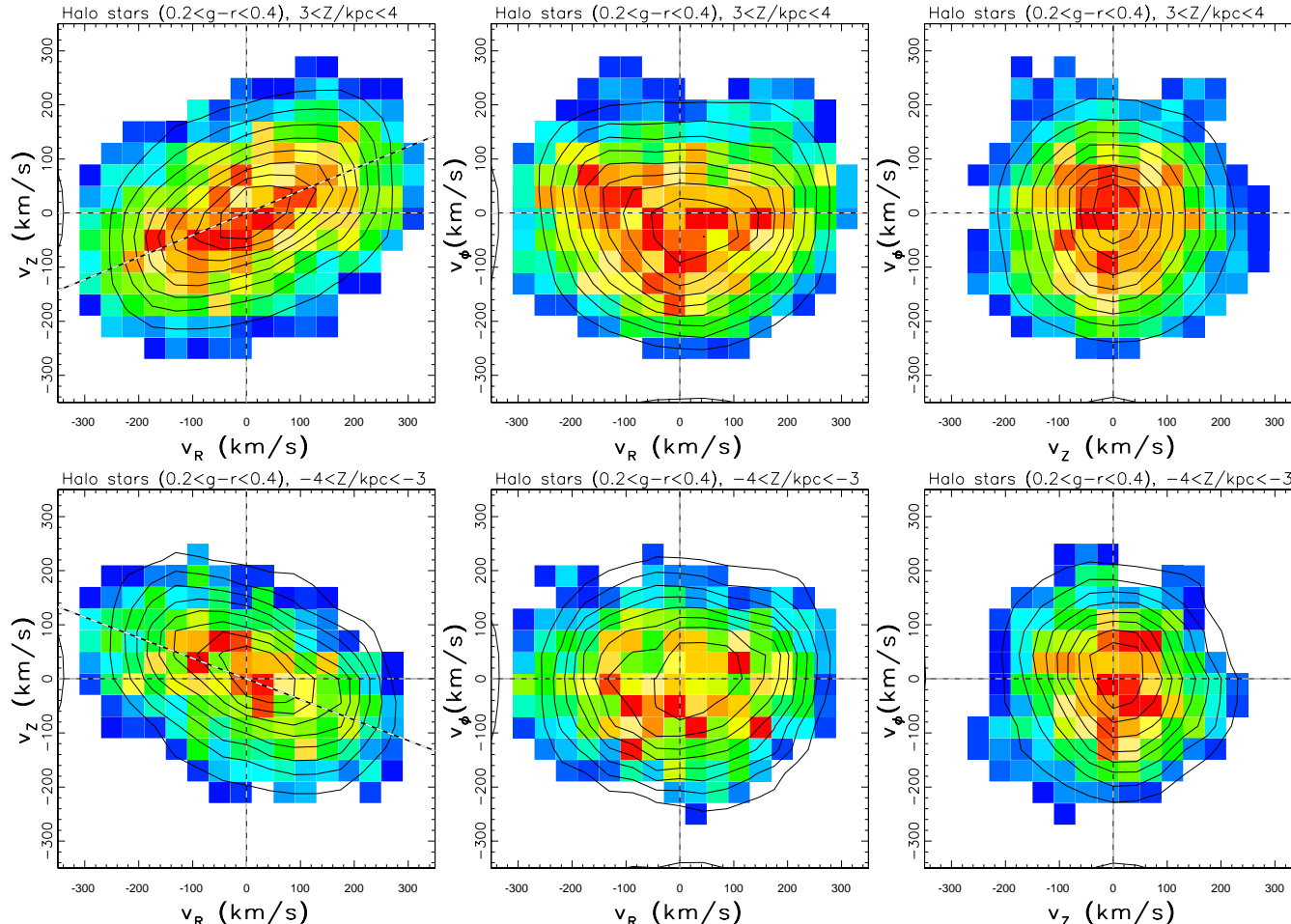
using disk star kinematics from SDSS (note the ten times better precision than in Bahcall's result).

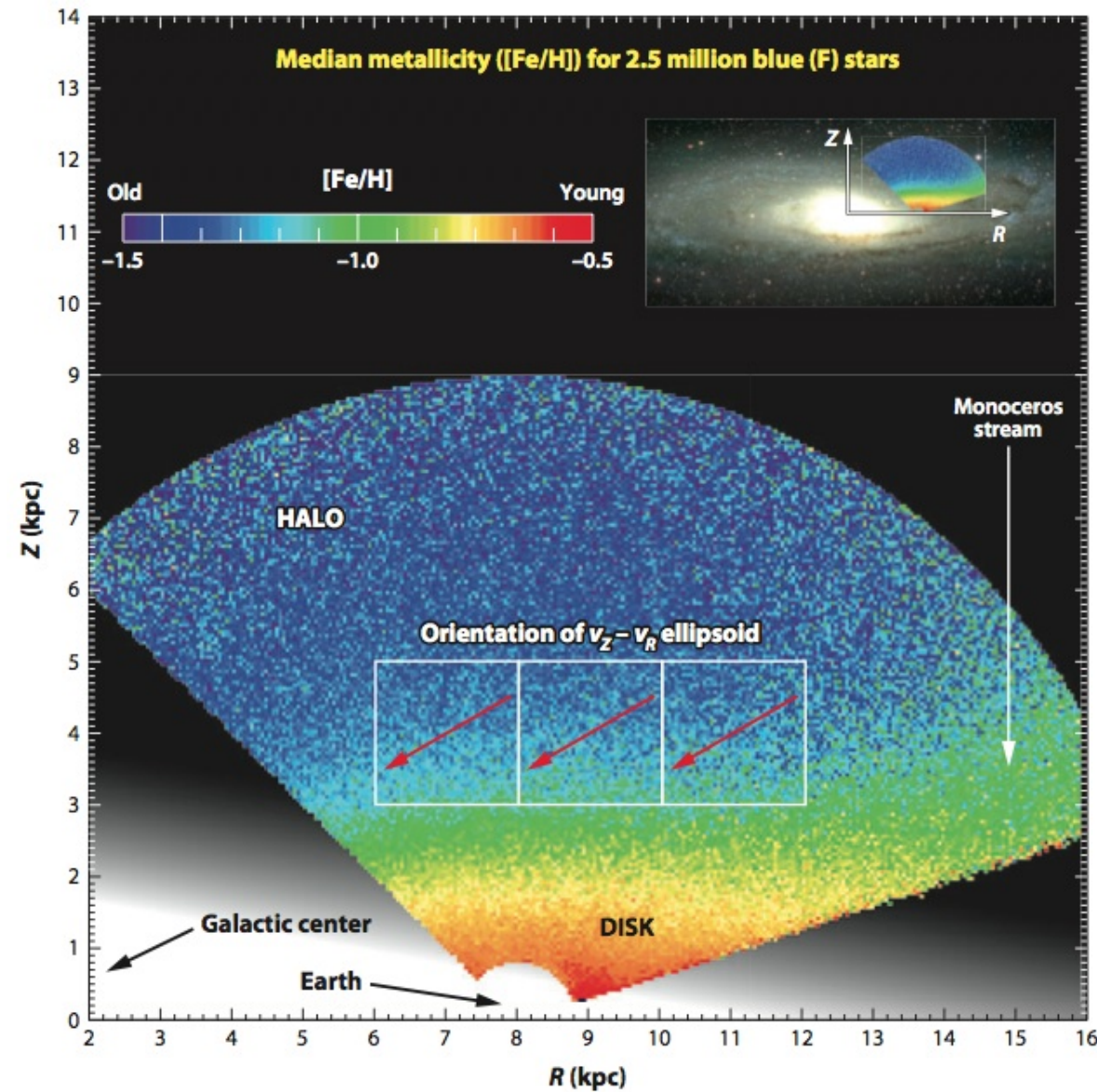
The Bovy & Tremaine result represents a statistically significant (probably the first one) dynamical detection of dark matter in the solar neighborhood!

But note that it is only a  $\sim 10\%$  effect (recall a factor of 3 effect from the Loebman et al. 2014 study).

# Halo Velocity Ellipsoid Tilt

- Three two-dimensional projections of the velocity distribution for two subsamples of candidate halo stars ( $[Fe/H] < -1.1$ ) with  $6 < R/\text{kpc} < 11$ , and  $3 < Z/\text{kpc} < 4$  (top) and  $-4 < Z/\text{kpc} < -3$  (bottom)
- The  $v_Z$  vs.  $v_R$  velocity ellipsoid is aligned with spherical coordinate system (Bond et al. 2010). Confirms results of Smith et al. (2009) over 30 times larger area.





A comparison of counts,  
metallicity distribution and  
kinematics.

- The arrows illustrate the variation of the ellipsoid orientation, which **always points toward the Galactic center!**
- This measurement can be used to infer the shape of gravitational potential (Loebman et al. 2012, ApJ 758, L23, see Lecture 10).

# A smooth global kinematic model is possible...

- Overall kinematic behavior can be captured by a simple model

18

BOND ET AL.

Vol. 716

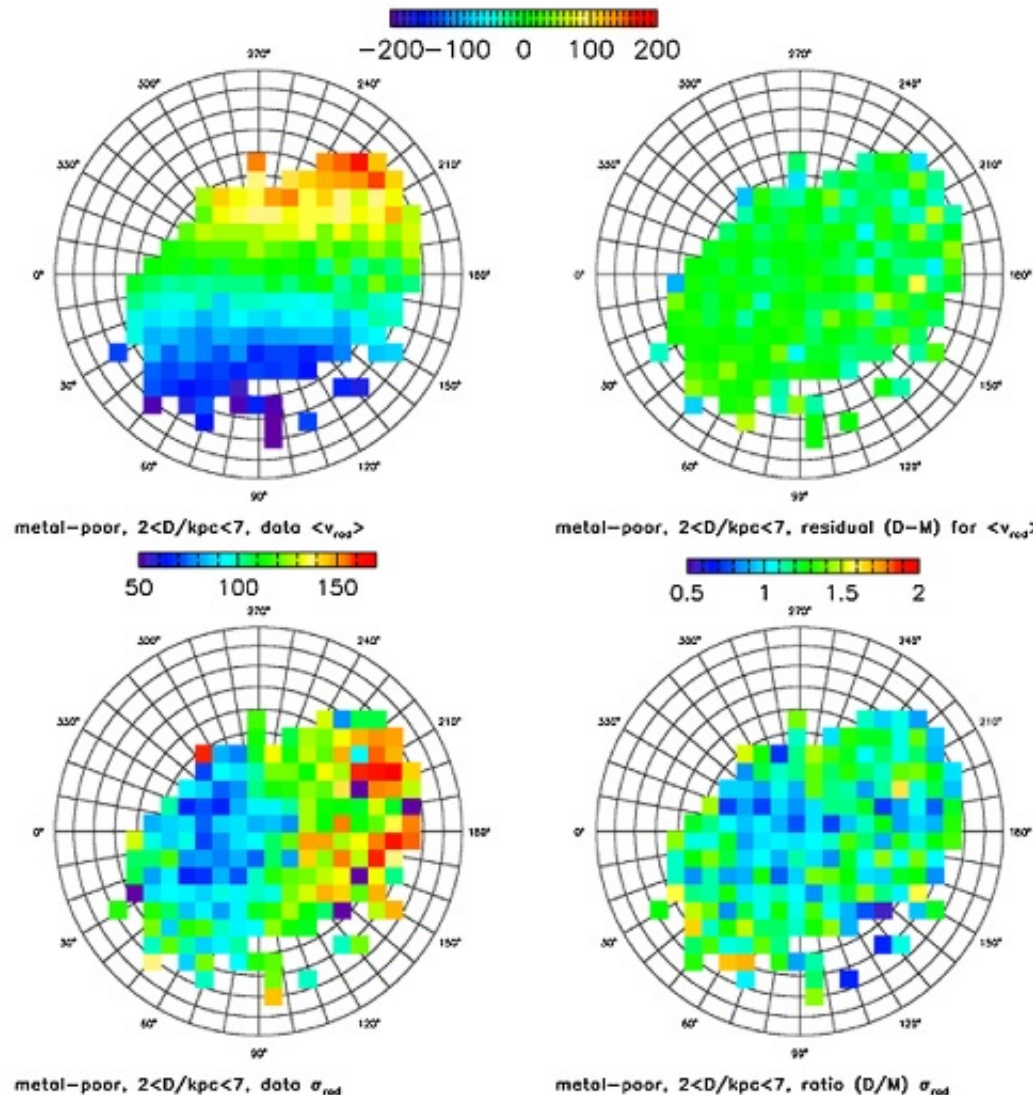


**Figure 16.** Comparison of medians and dispersions for the measured and modeled radial velocities of 20,000 blue ( $0.2 < g - r < 0.4$ ) halo stars (spectroscopic  $[\text{Fe}/\text{H}] < -1.1$ ) at distances,  $D = 2 - 7 \text{ kpc}$ , and  $b > 20^\circ$ . The top-left panel shows the median measured radial velocity in each pixel, color-coded according to the legend shown at the top (units are  $\text{km s}^{-1}$ ). The top-right panel shows the difference between this map and an analogous map based on model-generated values of radial velocity, using the same scale as in the top-left panel. The bottom-left panel shows the dispersion of measured radial velocities, color-coded according to the legend above it. The bottom-right panel shows the ratio of this map and an analogous map based on model-generated values of radial velocity, color-coded according to the legend above it. When the sample is divided into 1 kpc distance shells, the behavior is similar.

# A smooth global kinematic model is possible...

- for both low- and high-metallicity components

22

BOND ET AL.

Vol. 716

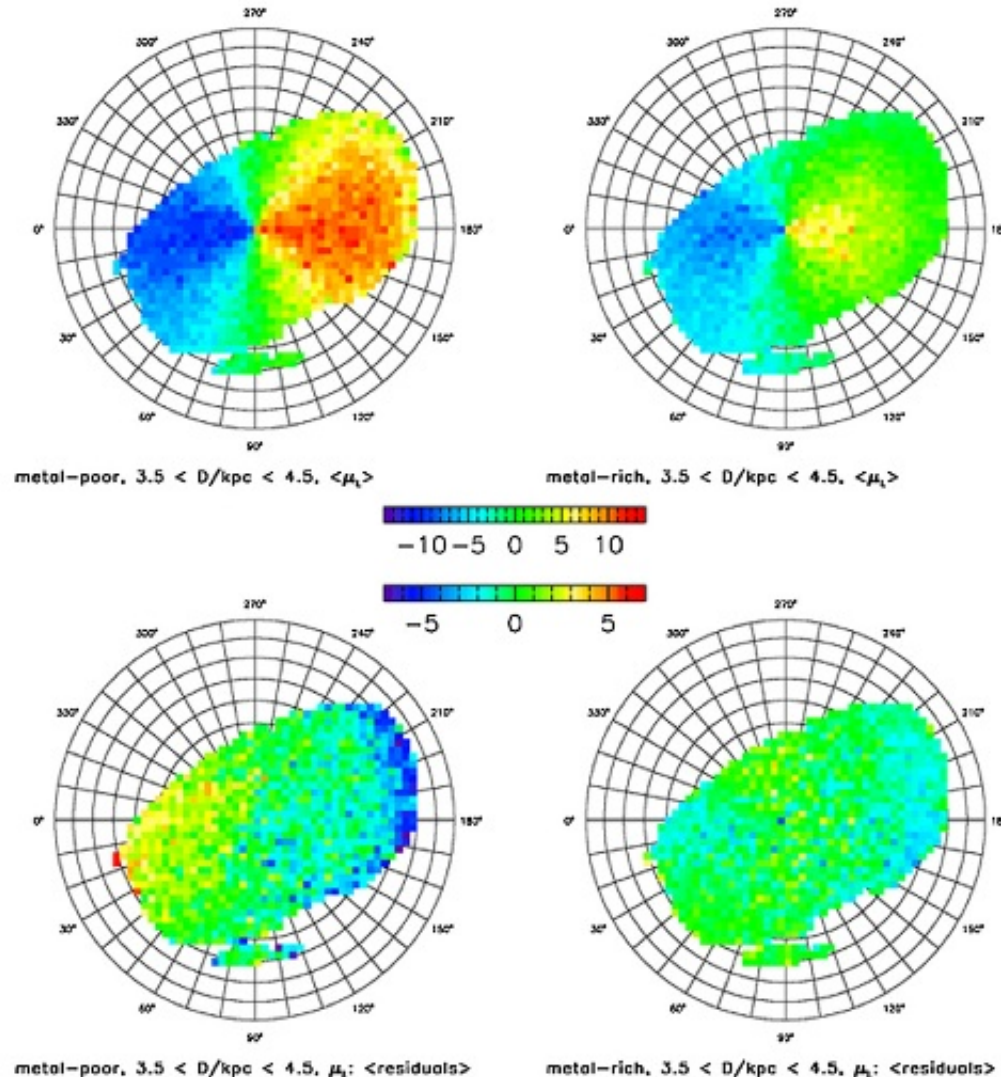


**Figure 20.** Similar to Figures 17 and 19, except that the behavior of high-metallicity (left) and low-metallicity (right) stars is compared in a single distance bin (3.5–4.5 kpc). The top two panels show the median longitudinal proper motion, and the two bottom panels show the median difference between the observed and model-predicted values. An analogous figure for the latitudinal proper motion has similar characteristics.

# Empirical Model for Mock Catalogs: **Galfast**

- Web service by Mario Jurić based on smooth spatial, metallicity and kinematics distributions measured by SDSS
- Available from [www.mwscience.net/galfast](http://www.mwscience.net/galfast)
- A valuable tool when searching for substructure in data, or comparing to theoretical models
- For example, can easily make mock catalogs for surveys such as SDSS, SkyMapper, Pan-STARRS, Gaia, and LSST
- Additional very popular codes: Besancon and Trilegal.

The screenshot shows the Galfast web interface. At the top, there's a navigation bar with links for File, Edit, View, History, Bookmarks, Tools, and Help. The address bar shows the URL <http://hybrid.mwscience.net/galfast/?jobid=4>. The main content area has several sections:

- Job Options:** Includes fields for Description (Flux limited/volume cut LSST samp), E-mail for notification (majuric@gmail.com), Send e-mail on completion (unchecked), Random seed (42), Output in FITS format (checked), Skip Q/A plot generation (unchecked), and Make this a template for new jobs (unchecked).
- Model:** Maximum stars to generate (50e6).
- Density Components:** A section for "Exp Disk and Power Law Halo (model\_5cc3d9.conf)". It includes a dropdown menu for Model type (Exp Disk and Power Law Halo), an Enabled checkbox (checked), Solar offset ( $Z_\odot$ ) (24), Thin disk parameters ( $\rho_0, L_1, H_1$ ) (1, 2150, 245), Thick disk parameters ( $f_D, L_2, H_2$ ) (0.13, 3261, 743), Halo parameters ( $f_H, \rho_H, q$ ) (0.0051, 2.77, 0.64), Cutoff radius ( $r_{\text{cut}}$  in pc) (100000), Luminosity function band ( $M_{-X}$ ) (LSSTz), and Luminosity function,  $\Phi(M_{-X})$  (MzLF.lf.txt).
- Observed area:** A section with an Add button.
- Double-exponential density profile (with Jurić et al. 2008, defaults):** Describes the density in terms of three components: thin and thick disks (double-exponentials), and a power-law halo. It provides mathematical formulas for each component:
  - $\rho(R, Z) = \rho_{\text{thin}}(R, Z) + \rho_{\text{thick}}(R, Z) + \rho_H(R, Z)$
  - $\rho_{\text{thin}}(R, Z) = \rho_0 e^{\frac{R_\odot}{L-1}} \exp\left(-\frac{R}{L_1} - \frac{Z+Z_\odot}{H_1}\right)$
  - $\rho_{\text{thick}}(R, Z) = f_D \rho_0 e^{\frac{R_\odot}{L_2}} \exp\left(-\frac{R}{L_2} - \frac{Z+Z_\odot}{H_2}\right)$
  - $\rho_H(R, Z) = \rho_0 f_H \left(\frac{R_\odot}{\sqrt{R^2 + (Z/q_H)^2}}\right)^{n_H}$It also mentions a Log file (output.log), Results (Mock catalog: sky.fits (121 MB)), and a note that the density is truncated to zero beyond  $r_{\text{cut}}$  galactocentric distance.
- Plot:** A scatter plot titled "Solar offset  $Z_\odot$ : The offset of the Sun from the Galactic plane (parsecs)." The y-axis is labeled "Median Tracer" and ranges from -0.3 to -0.29. The x-axis is unlabeled. A vertical line is drawn at approximately -0.295.

At the bottom, there are buttons for Save changes, Queue, Clone, Remove, Clean, Delete, and Done. A help pane is open on the right side.

## Summary of Metallicity/Kinematics Results

- Clumps/overdensitiesstreams are an integral part of Milky Way structure, both for halo and disk components; the kinematics and metallicity distributions are exceedingly complex.
- Nevertheless, it is possible to construct a reasonably good model for the smooth global behavior (Bond et al. 2010)
- The rotational lag (velocity shear) and metallicity distribution for disk stars are smooth functions of  $Z$
- The halo velocity ellipsoid is invariant in spherical coordinates (within 10 kpc or so).

SDSS has revolutionized studies of the Galactic structure;

Gaia and LSST will do even better! (the last lecture)